https://doi.org/10.5194/os-2022-16
Preprint. Discussion started: 1 April 2022

Ocean Science
Discussions
Open Access
EGU

The role of oceanic heat flux in reducing thermodynamic ice growth in Nares Strait and promoting earlier collapse of the ice bridge

Sergei Kirillov[1], Igor Dmitrenko[1], David G. Babb[1], Jens K. Ehn[1], Nikolay Koldunov[2], Søren Rysgaard[1,3,4], David Jensen[1], and David G. Barber[1]

[1]Centre for Earth Observation Science, University of Manitoba, Winnipeg, Manitoba, Canada
[2]Alfred Wegener Institute, Bremerhaven, Germany
[3]Arctic Research Centre, Aarhus University, Aarhus, Denmark
[4]Greenland Institute of Natural Resources, Nuuk, Greenland

Correspondence to: Sergei Kirillov (sergei.kirillov@umanitoba.ca)

Abstract. The ice bridge in Nares Strait is a well-known phenomenon that affects the liquid and solid freshwater flux from the Arctic Ocean through the strait and controlling the downstream North Water polynya in the northern Baffin Bay. Recently, the ice bridge has been in a state of decline, either breaking up earlier or not forming at all, and thereby increasing the sea ice export out of the Arctic Ocean. The decline of the ice bridge has been ascribed to thinner and therefore weaker ice from the Arctic Ocean entering Nares Strait, however local forcing also affects the state of the ice bridge and thereby influences when it breaks up. Using a variety of remotely sensed data we examine the spatial patterns of sea ice thickness within the ice bridge; highlighting the presence of negative ice thickness anomalies on both the eastern and western sides of the Strait, and identifying a recurrent sensible heat polynya that forms within the ice bridge near Cape Jackson in northwestern Greenland. Using the sea ice-ocean model FESOM2, we then attribute these ice thickness anomalies to upwelling of warm modified water of Atlantic origin (mAW) that reduces thermodynamic ice growth throughout winter. The consequently weaker and thinner areas within the ice bridge promote instability and the earlier break up. This work provides new insight into the Nares Strait ice bridge, and highlights that a combination of thinner ice and warmer mAW entering the Strait is contributing to its decline.

1. Introduction

Nares Strait is a narrow waterway between Ellesmere Island and Northwestern Greenland that connects the Arctic Ocean and northern Baffin Bay (Fig. 1). This strait represents one of the major gates through which cold and fresh Arctic seawater and sea ice discharge into north Atlantic (Kwok, 2005; Beszczynska-Möller et al., 2011; Münchow, 2016). The southward ice and water flow is maintained by persistent orographically channeled winds (Ito, 1982; Samelson et al., 2006) and a sea level gradient between the Lincoln Sea and Baffin Bay (Shokr et al., 2020). The situation changes dramatically with the formation of the ice bridge at the northern end of Smith Sound that blocks southward ice drift during winter. The presence of the ice bridge significantly reduces the annual sea ice transport through Nares Strait. An average ice export of ~141 km^3 per year is about half of that exported during years when the ice bridge fails to form (Kwok et al., 2010). The ice bridge also helps prevent the loss of the thick, old ice from the Last Ice Area (Moore et al., 2019), located north of Ellesmere Island and Greenland, by hindering its transport south, where it in turn may affect navigation and marine industry (Barber et al., 2018). Generally, the composition of the ice bridge can be described as a mix of first year ice (FYI), multiyear ice (MYI) and a minor contribution of ice bergs. Kwok (2005) reported that MYI comprises between 18% and 75% of the total ice area drifting through Nares Strait and accounts for most of the total ice volume flux (Kwok et al., 2010). Under-ice sonar measurements in Kennedy Channel showed the modal peak of ice drafts of 2.0–2.1 m throughout winter season including the periods of ice growth and melt (Ryan and Münchow, 2017). Based on a limited high-

https://doi.org/10.5194/os-2022-16
Preprint. Discussion started: 1 April 2022

resolution satellite altimetry dataset for Nares Strait in January 2020, Kirillov et al. (2021) demonstrated that the ice bridge mainly consisted of relatively thick ice with a pronounced peak in the fraction of sea ice with a draft between 2.6–2.8 m.

The period when the strait is impenetrable for ice transport depends on the timing of ice bridge formation and break-up. The ice bridge forms typically between late-October and early-April and breaks up in June-July (Kwok, 2010; Vincent, 2019). Kirillov et al. (2021) demonstrated that drifting ice has a higher likelihood to consolidate under a specific combination of favorable atmospheric and oceanic conditions. Analysis of 16 bridge formations during the past two decades revealed that consolidation occurred at cold air temperatures (less than -15°C), around neap tide, and during a cessation or even reversal in the prevailing north-northeasterly winds in the strait. However, the authors also showed that the combination of favorable forcing did not necessarily result in bridge formation. For instance, the bridge failed to form during five recent winters (i.e., 2007, 2009, 2010, 2017 and 2019), although favorable atmospheric and oceanic conditions often met the criteria of consolidation. That bridgeless years only occurred during last 15 years underscore a general shortening of bridge existence period and point to changes in environmental conditions. Based on AVHRR satellite data from 1979 to 2019, Vincent (2019) reported on a recent trend towards later formation and earlier breakup of the ice bridge.

The formation of the Nares Strait ice bridge also contributes to the formation and maintenance of the North Open Water (NOW) polynya. Being the largest recurring latent heat (wind-driven) polynya in the Canadian Arctic (Tamura and Ohshima, 2011; Preußer et al., 2019), the NOW has significant impacts on oceanographic, atmospheric and biological conditions and processes in northern Baffin Bay (Dumont et al., 2010). The high biological productivity supported by NOW is of critical importance to Inuit that hunt and fish in the area (Hastrup et al., 2018; QIA 2020). Despite NOW is believed to be one the most studied polynya, it is the sensible heat polynyas associated with an impact of relatively warm modified Atlantic water (mAW) underlying the cold surface mixed layer that are more common in the Canadian Arctic (Hannah et al., 2009). Most of these polynyas are formed in the narrows where strong tidal and mean currents facilitate upward heat transfer from depth (Hannah et al., 2009). In addition to the sensible heat polynyas, which are visible at the surface, there are numerous so-called “invisible polynyas”, also associated with the upward heat flux from below, in the Canadian Arctic where the ice cover is appreciably thinner than the surrounding ice (Melling et al., 2015). Covered with thinner ice, these areas are evident for earlier break up and, therefore, may also be a factor facilitating a collapse of landfast ice cover in summer. So far, the consideration of polynyas in Nares Strait has been mainly limited to latent NOW and, to a less extension, to Lincoln Sea polynya (Barber and Massom, 2007). The sensible heat polynyas in Nares Strait are relatively small and less studied, but still interesting as they form within a stable landfast area and are associated with ocean heat flux from below. Those polynyas are located in the Bache Peninsula Region at the eastern side of Ellesmere Island (Schledermann, 1980; Hannah et al., 2009) and seem to be local hot spots as they evidence for nearby prehistoric settlements extending back from 2500 to 3000 years (Schledermann, 1978).

Another sensible polynya forms at Cape Jackson in the central part of the bridge (at ~80° N) – to our best knowledge the northernmost sensible polynya on our planet. Although some historical materials and papers have mentioned this polynya (Kane, 1856; Vibe, 1950), its existence have remained hidden from a wide scientific community and no special studies around it have been conducted. The first written account of this polynya was found in the report of the Second Grinnell Expedition led by Dr. Elisha Kane, which was looking for Sir John Franklin’s expedition. From the words of Mr. Morton and Hans Hendric whose dog sled party reached this area in June 1853, Dr. Kane made the followed record:

“*June 21, Wednesday. They stood to the north at 11.30 p.m., and made for what Morton thought a cape [Cape Jackson], seeing a vacancy between it and the West Land. The ice was good, even, and free from bergs, only two or three being in sight… They reached the opening seen to the westward of the cape by Thursday, 7 a.m.*” (Kane, 1856; p. 284).

It follows by a description of substantially deteriorated ice in the vicinity of the discovered open water:

https://doi.org/10.5194/os-2022-16
Preprint. Discussion started: 1 April 2022

"*The ice was weak and rotten, and the dogs began to tremble. Proceeding at a brisk rate, they had got upon unsafe ice before they were aware of it. … The only way to induce the terrified, obstinate brutes to get on was for Hans to go to a white-looking spot where the ice was thicker, the soft stuff looking dark; then, calling the dogs coaxingly by name, they would crawl to him on their bellies. So they retreated from place to place, until they reached the firm ice they had quitted. A half-mile brought them to comparatively safe ice, a mile more to good ice again.*".

Several years later, in the middle of May 1861, expedition of Hayes approached Kennedy Channel by Ellesmere coast. Although he likely failed to reach the entrance to the channel, the following observation was made close to cape Frazer:

"*To the north-east the sky was dark and cloudy, and gave evidence of water; and Jensen was not slow to direct my attention to the "water-sky"* (Hayes, 1867; p. 395).

On the other hand, Knut Rasmussen, who stepped over Morton's and Hendric's footprints near Cape Jackson earlier in the season (end of April) of 1917, did not report any open water there (Rasmussen, 1921; p. 61-65).

Although the ocean-derived character of polynya at Cape Jackson is a matter of fact, the question about heat source remains unanswered because so little is known about an ocean state beneath the ice bridge between its formation and break up. The consolidation of sea ice modifies the structure of water flow through the strait leading to a shift of southward geostrophic flow from the middle to the western side of the strait (Rabe et al. 2010; Rabe et al. 2012; Shroyer et al. 2015). However, scarce velocity measurements limited mainly to the Kennedy Channel do not allow to evaluate these results confidently for the entire strait and identify the process maintaining water at Cape Jackson ice-free during winter. This study intends to partially fill these gaps and shed light on the ice-ocean interaction under the bridge during winter and the role of this interaction in formation of polynya at Cape Jackson and other yet unknown invisible polynyas in Nares Strait.

The overarching goal of this paper is to demonstrate an impact of ocean heat on the sea ice in Nares Strait and examine its possible role in breaking up the ice bridge. The paper is organized as follows. In the followed section, we make a short overview of observational evidence of polynya at Cape Jackson in historical records. In Section 2, we describe datasets used in this study. The results obtained from the remote sensing data on sea ice in Kane Basin are presented in Section 3.1. In the next section, we show the results of 1-D simulations of ice growth in Peabody Bay. And the description of ocean circulation and water mass structure in Kane Basin obtained with FESOM-2 numerical model is given in Section 3.2. The findings are summarized and discussed in Section 4, followed by main conclusions in Section 5.

2. Data and methods

2.1 Satellite imagery

In this study, we used remote sensing data from different satellites. First, the true color imagery from the Moderate Resolution Imaging Spectroradiometer (MODIS) and Sentinel-2 were used to identify the ice-free areas in Nares Strait. MODIS was first launched in 1999 on board the Terra satellite, with the second sensor launched in 2002 aboard the Aqua satellite. In addition to the daily global composites of the true color band composition (Bands 1, 3 and 4; spatial resolution 250 m), the MODIS sea surface brightness temperature (T_b, band 31 mid-infrared; spatial resolution 1 km) was also used. T_b is calculated from the top-of-the-atmosphere radiances and shows the relative temperature difference between open water, and thick and thin sea ice. The Sentinel-2A and 2B satellite with high-resolution multispectral optical imager (spatial resolution 10 m) onboard were launched in 2015 and 2017, respectively, as part of the European Space Agency's Copernicus mission. The usage of both optical and infrared products is considerably limited by the presence of clouds. In this research, we used the images obtained during clear-sky conditions.

https://doi.org/10.5194/os-2022-16
Preprint. Discussion started: 1 April 2022

The daily averaged sea ice brightness temperatures from the 89V GHz channel and snow depths obtained by Advanced Microwave Scanning Radiometer (AMSR) not interfering with clouds were also used. AMSR instruments are carried by the Aqua satellite (AMSR-E) and the Japan Aerospace Exploration Agency (JAXA) Global Change Observation Mission – Water 1 (GCOM-W1) satellite. Both datasets are provided by the National Snow & Ice Data Center (NSIDC) at 6.25 km spatial resolution for temperatures (Cavalieri et al, 2014; Meier, et al, 2018) and 12.5 km for snow depths (Tedesco & Jeyaratnam, 2019).

2.2. Ice surface elevation data

In addition to satellite imagery, surface elevation data from the recently launched Ice, Cloud and Land Elevation Satellite (ICESat-2, launched in October 2018) were used to characterize the ice surface elevations in Nares Strait. The elevations are acquired by the Advanced Topographic Laser Altimeter System (ATLAS) instrument that counts individual photons in short segments along three pairs of strong (segment length of ~15 m) and weak (~60 m) beams. For this study we used ATL07/L3A v.3 product that contains the elevations for sea ice/snow and open water (Kwok et al, 2020a). In some particular cases, the ice-free area within the polynya at Cape Jackson was used as a reference level for an estimation of absolute ice/snow freeboard heights in vivinity of polynya. Although the absolute surface heights over narrow bridges may be determined via linear interpolation of sea surface heights measured at the opposite sides of bridge (Babb et al., in press), this approach requires ICESat tracks crossing a bridge from edge to edge what does not work for Nares Strait. Therefore, considering the lack of leads and, therefore, sea surface height references within the ice bridge, we introduced a new method based on finding the ATL07 along-track anomalies of ice heights ($\tilde{h}$). The anomalies are calculated relative to mean height of any ascending or descending track crossing the bridge between 55-76°W and 78.25-82.5°N, and then averaged into 1x1 km grid to obtain the maps of relative surface heights.

Although ATL07 data are manifested to be adjusted for geoidal/tidal variations and inverted barometer effects, they may still contain unknown uncertainties related to the regional synoptic variability of sea level associated with wind forcing and/or with ocean dynamics. However, the presence of immobilized ice and relatively short along-track distances from coast to coast within Kane Basin allow to suggest that spatial variations of these uncertainties are relatively small. Another type of uncertainty related to the estimation of ice surface height and, hence, thickness from ICESat-2 data is connected to the generally unknown snow depths. The existing climatology or estimates of snow depths in the Arctic either do not cover the study area (Warren et al., 1999; Kwok et al., 2020b) or seem to be too coarse to provide data in Nares Strait (Rostosky et al., 2018; Glissenaar et al., 2021). Using DMSP/SSM/I-SSMIS brightness temperatures, Landy et al. (2017) reported >0.3 m mean snow depth in Kane Basin. However, as we will show later, this height seems to be overestimated and the more modest mean snow depth of 19±2 cm in Peabody Bay obtained from mean March-April AMSR2 data (Tedesco & Jeyaratnam, 2019) is thought to be more reliable estimate.

2.3. Modelling

The unstructured-grid Finite volumE Sea ice Ocean Model version 2 (FESOM2) (Danilov et al., 2017; Scholz et al., 2019) was used for deriving high-resolution water dynamics in Nares Strait. The model's sea ice component is discretized on the same unstructured grid as the ocean component. It can faithfully reproduce sea ice observations, including sea ice linear kinematic features when using high model resolution (Koldunov et al., 2019; Wang et al., 2016). We used the same model setup as Wang et al. (2020) with horizontal resolution of 30 km in the global ocean, except for the Arctic Ocean, where the resolution is 1 km. In the vertical, 70 z levels are used. The model was driven by the atmospheric reanalysis fields from JRA55-do v.1.4 (Tsujino et al., 2018). It was initialized from PHC3 climatology starting from the year 2000 and has been run for 10 years (the only hi-res output yet available at the moment). Here we analyze the last five model years from 2006 to 2010.

https://doi.org/10.5194/os-2022-16
Preprint. Discussion started: 1 April 2022

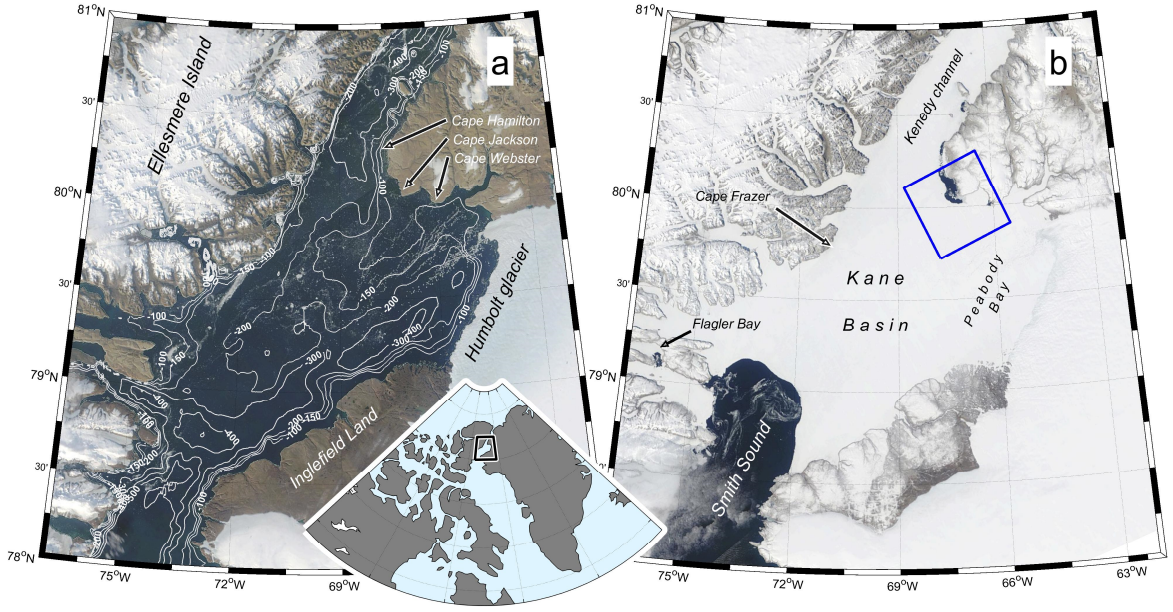

Figure 1: (a) The bathymetry of the central part of Nares Strait with contours corresponding to 100, 150, 200, 250 and 300 m isobaths. (b) The true color image of the sensible polynya at Cape Jackson on 6 June 2021. The blue square borders a region shown in Figure 2.

To assess the quality of the model in this region, we compared the thermohaline structure and along-channel current speeds in the Kennedy Channel where an intensive mooring observation program was conducted in 2003-2006 and 2007-2009 (Münchow and Melling, 2008; Münchow, 2016). It was found that both vertical and cross-channel distributions of temperature/salinity and current velocities in FESOM2 simulations generally have good agreement with the mooring records in this region (Münchow & Melling, 2008; Rabe et al., 2010; Münchow, 2016). However, despite a good correspondence of model results and observations in the Kennedy Channel, we have to admit that the largely uncertain bathymetry of Kane Basin (and especially its eastern part) combined with an enormous number of floating and grounded icebergs originated from the Humboldt glacier may significantly affect quality of model simulations in this area.

2.4. Atmospheric forcing and 1-D ice growth model

The 6-hourly records of 2 m air temperature, wind speed and humidity in Kane Basin were taken from the ERA-5 global reanalysis database (Copernicus Climate Change Service (C3S), Hersbach et al, 2020) and used to run a 1-D sea ice growth model. The model allows for ocean heat flux and snow accumulation, and may also effectively reproduce flooding, which is associated with a large snow load and leads to the formation of a snow-ice layer (Kirillov et al., 2015). The model was run with different snow accumulation rates and ocean heat flux from 17 December 2019 to 30 April 2020. Two principal scenarios of sea ice growth were simulated: (1) under different but invariable ocean heat fluxes and snow accumulation rates to simulate the ice growth in the middle of Peabody Bay, and (2) without snow cover directly at Cape Jackson. To avoid computational issues, the snow was added in the model discretely every 15 days instead of a continual accumulation.

Air temperatures were additionally used to quantify the annual number of freezing-degree days during winter that is calculated as the sum of the daily degrees below the freezing point of seawater (-1.8 °C). The freezing-degree days (FDD) were used to roughly

https://doi.org/10.5194/os-2022-16
Preprint. Discussion started: 1 April 2022

estimate the thermodynamic growth of sea ice through the empirical relationship connecting FDD and ice thickness. The most often used parameterization of ice growth under average snow conditions in the Arctic was introduced by Lebedev (1938) in a form of $h(m)=0.0133\times FDD^{0.58}$, although other possible parameterizations also exist (Bilello, 1961) and were considered in this research.

3. Results

3.1. Identifying the polynya at Cape Jackson

MODIS imagery confirm that a polynya is present every winter at Cape Jackson within the ice bridge since MODIS observations begain in 2000. The snapshot true color images in Fig. 2 show the state of ice cover in vicinity of the cape in May when the air temperatures are still negative with a climatic mean varying form -12 °C (2 May) to -7 °C (20 May; ERA5). However, the open water is often evident starting from early March (not shown) when the mean climatic air temperatures are below -25 °C**.** Although the configuration of dark spots corresponding to open water or thin sea ice in Fig. 2 varies from year to year, the high persistance in their positioning suggests the existance of a highly persistent ocean heat flux that exceeds the intense loss of heat to the atmosphere. The presence of sensible heat polynya at Cape Jackson is also evident in sea surface brightness temperatures in January-February (MODIS T_b, not shown), although polynya signatures are less clear in those images because of their lower spatial resolution. The higher values of T_b in vicinity of Cape Jackson may indicate either the ice-free surface or thinner ice above the invisible polynya.

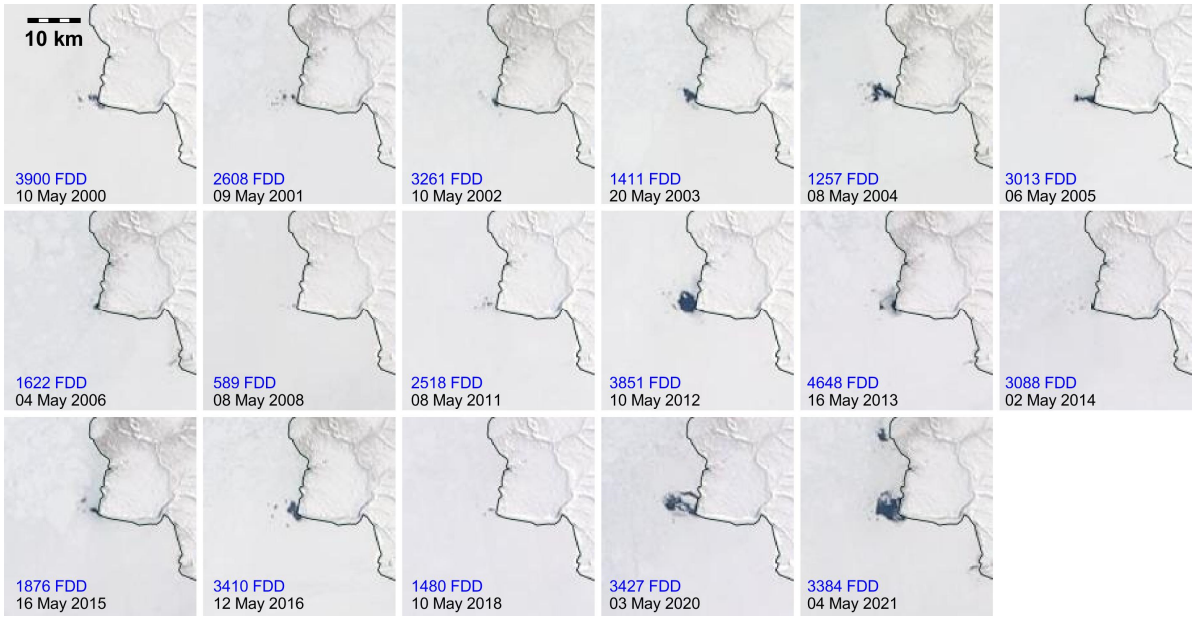

Figure 2: The presence of sensible heat polynya at Cape Jackson during winters when ice bridge in Nares Strait formed between 2000 and 2021. Blue numbers correspond to the sum of freezing degree days (FDD) from a corresponding date of bridge formation (see Kirillov et al., 2021) to 30 April. Each panel is 37.5 x 37.5 km.

ICESat2 transects confirm the presence of thinner ice in the vicinity of Cape Jackson. Figure 3 shows the heights along selected tracks crossing the polynya in March-May 2020 and in March-April 2021. Despite the presence of some short-scale variance, all

https://doi.org/10.5194/os-2022-16
Preprint. Discussion started: 1 April 2022

tracks begin to show a decrease in surface height 5 to 15 km away from the polynya. The distribution of surface heights from the selected scenes shows a modal height of 0.26 m, which corresponds to an estimated thickness of 2.42 m (for ρ_{ice} = 915 kg m^{-3}, ρ_{water} = 1025 kg m^{-3}) under snow-free conditions. This modal thickness, however, may be very sensitive to the accuracy of ICESat-2 measurements and more specifically to the offsets applied to each individual track in Fig. 3. An error of 1 cm in offsetting would alter the ice thickness by about 9 cm. Additionally the basic no-snow assumption introduces a much greater error in the estimated ice thickness. If 50% of the 0.26 m surface elevation is attributed to a snow layer with density of 300 kg m^{-3}, the resulting ice thickness decreases to 1.56 m and to 1.14 m if the snow-to-ice ratio above the sea level is 75-25%.

Beyond the central main part of polynya, there is also evidence of patches of thinner ice and open water surrounding that area (e.g. Fig. 3d), suggesting that there is some spatial variability of the ocean heat flux that maintains the polynya. The ICESat-2 tracks also demonstrate irregular spikes and elevated segments, which likely indicate the presence of thicker MYI ice, ridges or icebergs in this region.

https://doi.org/10.5194/os-2022-16
Preprint. Discussion started: 1 April 2022

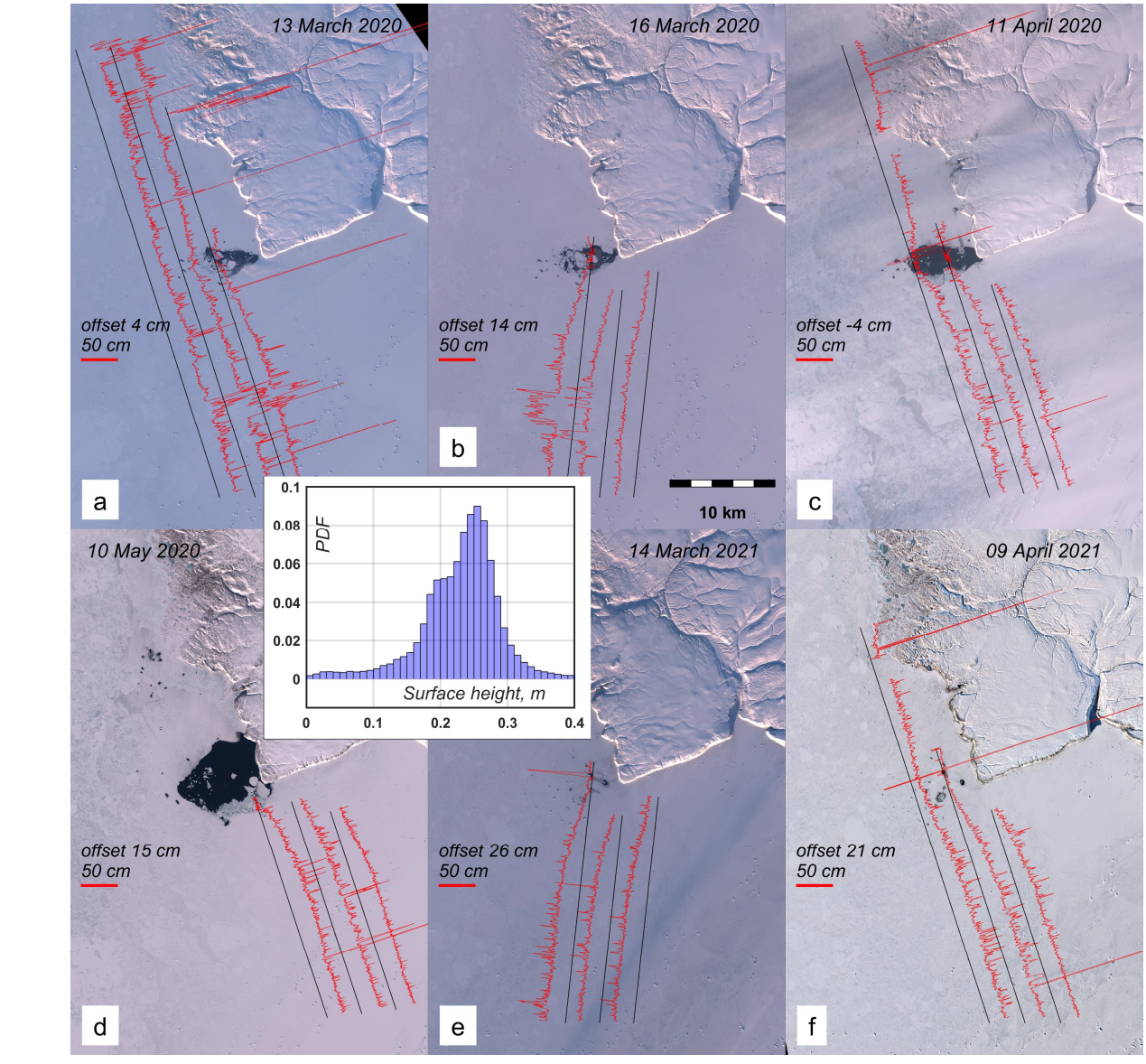

Figure 3: The ATL07 heights from 3 strong beams overlaid the Sentinel-2 image of polynya in March-May 2020 and in March-April 2021. The open water was used as a reference level to calculate the corresponding offsets for each subset. The inset histogram demonstrates the probability distribution of all heights shown in the panels a-f.

3.2. Basin-wide anomalies of sea ice thicknesses

Expanding from the area around Cape Jackson, Figure 4 represents the seasonally (January-April) averaged $\tilde{h}$ throughout Nares Strait in 2019, 2020 and 2021. In 2019, the bridge did not form, leaving the main channel of Nares Strait covered with mobile ice throughout winter, though landfast ice still formed across Peabody Bay in the eastern part of Kane Basin (Fig. 4a). The landfast ice edge represents a pronounced boundary dividing these two areas with different $\tilde{h}$ patterns. In the main channel, the anomalies are highly irregular and form a speckled pattern, whereas the anomalies in Peabody Bay form a consistent pattern with positive

https://doi.org/10.5194/os-2022-16
Preprint. Discussion started: 1 April 2022

anomalies in the southeast and negative anomalies to the northwest. A similar pattern of $\tilde{h}$ was observed over the landfast ice in Peabody Bay in 2020 (Fig. 4b), but not in 2021 (Fig. 4c). The anomalies in Peabody Bay vary mainly between -5 and +5 cm, although elevated negative anomalies were observed along the northern coast of Peabody Bay during all 3 winters. These elevated anomalies are mainly constrained between Cape Jackson and Cape Webster, although they can be traced further along the coast in both northwestern and eastern directions. The values of $\tilde{h}$ of -15 to -10 cm in this coastal zone are about two times smaller than anomalies found along the individual ICESat-2 tracks at Cape Jackson in March-May (Fig. 3). This discrepancy is partly attributed to the seasonal averaging of data used to compute $\tilde{h}$, but combining anomalies obtained from ascending and descending ICESat-2 tracks with different along-track regional means may also result in smoothing of spatial anomalies presented in Fig. 4. Another interesting feature observed during winters with a bridge is the presence of persistent negative anomalies of $\tilde{h}$ along the western coast of Nares Strait (Fig. 4b, c). These anomalies are not visually associated with any polynyas at least until late summer.

The difference in surface height anomalies between the southeastern and northwestern parts of Peabody Bay is supported by a similar difference in the observations of T_b. The mean AMSR temperatures in March for all three years are shown in Fig. 5 and highlight the possibility of presence of warmer (thinner) ice in the northwest compared to colder (thicker) ice in the southwest. In 2019, the temperature contrast between these regions is slightly stronger because the northwestern part of Peabody Bay remained covered with pack ice. Additionally, AMSR data did not reveal temperature anomalies in the area where negative $\tilde{h}$ anomalies are observed along the coast in western Nares Strait (Fig. 5b,c).

https://doi.org/10.5194/os-2022-16
Preprint. Discussion started: 1 April 2022

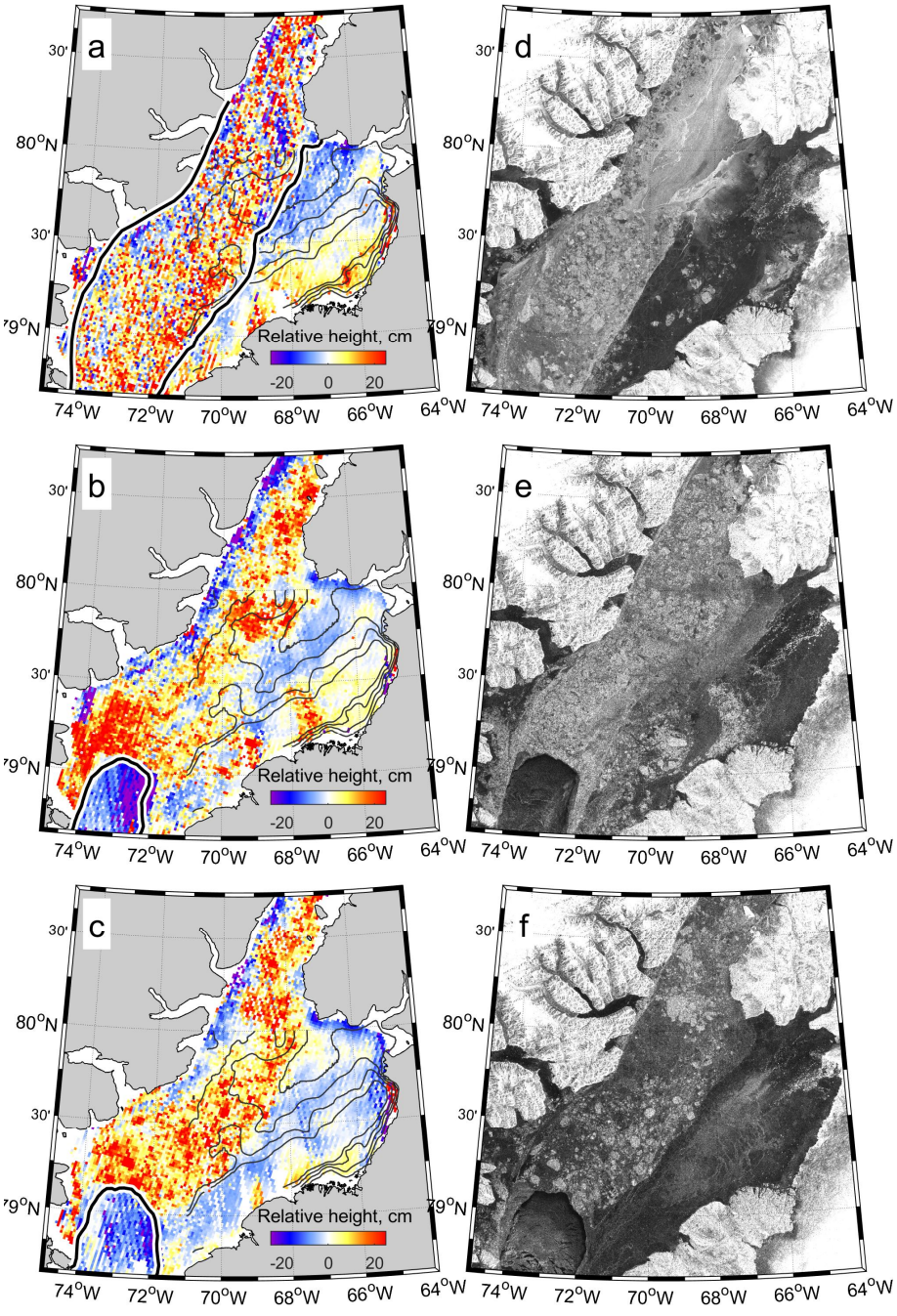

240

Figure 4: (a-c) The along-track anomalies of ATL07 heights averaged over 1x1 km cells in January-April 2019 (a), 2020 (b) and 2021 (c). The thick black lines correspond to approximate positions of landfast ice edge during these winters. (d-e) Sentinel-1 SAR images from January 16 in the corresponding years.

https://doi.org/10.5194/os-2022-16
Preprint. Discussion started: 1 April 2022

The microwave SAR images presented in Fig. 4d-f help to characterize the composition of sea ice presented in Kane Basin and specifically in Peabody Bay during these three winters. It is clear that the sea ice in the bay consists mainly of smooth ice (black areas) with inclusions of ridges characterized by high backscatter and seen as white patches. The spatial distribution of ridges generally corresponds to the regions where elevated values of $\tilde{h}$ were found (e.g. Fig. 4b, e). Besides the irregular patches corresponding to ridges, the numerous grounded or ice-locked icebergs are also seen in the northeastern as linear white filaments in the vicinity of Humboldt glacier terminus (e.g. Fig. 4f and also Fig. 11). The generally smooth character of the ice surface suggests that sea ice in the bay is predominantly first year ice that has formed locally through thermodynamics. Contrary to this, the sea ice in the main channel is represented by a mix of relatively thin FYI (corresponding to dark areas) and thicker individual MYI floes (light spots) regardless of the presence of the ice bridge.

The results presented in Sections 3.1 and 3.2 generally support the hypothesis that it is the ocean heat flux that is responsible for formation of ice thickness anomalies in Nares Strait including polynya at Cape Jackson. In the next section, we will try to at least roughly estimate the intensity of this flux by calculating the ice growth with oversimplified empirical methods and through numerical simulation with 1-D thermodynamic model.

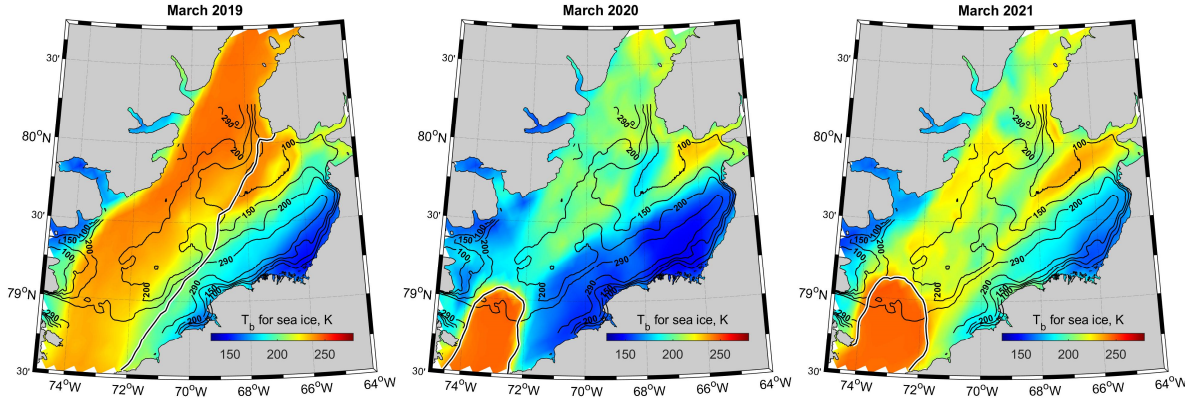

Figure 5: The ice surface temperatures in March from AMSR-E/AMSR-2 data in 2019, 2020 and 2021. The 100, 150, 200 and 250 m isobaths are shown in background, whereas the black lines in the right panel corresponds approximate positions of landfast ice edges.

3.3. Modeling of the thermodynamic ice growth in Peabody Bay

The timing of landfast ice formation in Peabody Bay varies from year to year, but generally occurs in October according to satellite data. The stable landfast ice first forms in the southeastern bay where hundreds of grounded icebergs from Humboldt glacier form several well-separated chains roughly aligned along isobaths. Most of these icebergs are grounded at the eastern slope of the mid-basin ridge and represent a “glue” that helps new thin ice bind together and stabilize. Although air temperatures in Kane Basin fall below zero in early September, the northwestern part of Peabody Bay, near Cape Jackson, can remain unfrozen until November or December. In winter 2019/20, for instance, this area was ice-free or covered with thin mobile ice until 17 December when the bridge formed. The amount of FDD from that date to the end of April reached 3427, giving an estimated ice thickness of 1.49 m under average snow conditions according to parameterization of Lebedev (1938). However, less snow may result in faster ice growth and greater resulting thicknesses. Using empirical relationship describing the ice growth under negligible amount of snow near Churchill (Canada) would give 1.86 m of ice at the end of winter (Graystone’s formula in Bilello, 1961). Another formula

https://doi.org/10.5194/os-2022-16
Preprint. Discussion started: 1 April 2022

proposed in Bilello (1961) for snow-free ice surface yields ice thickness of 2.00 m which is still smaller than 2.42 m thickness estimated from ICESat-2 data in the vicinity of Cape Jackson under the no-snow condition. The wide range of these ice thickness estimates underlines an importance of snow depth data for analysis of ICESat-2 surface heights and/or in-situ ice draft measurements. In addition, these empirical relationships do not take into account the ocean heat flux that may play a critical role in ice growth and conditions the existence of sensible heat polynyas.

To investigate the possible joint effect of snow and ocean heat flux on the observed spatial variations of surface heights in the vicinity of Cape Jackson, we applied the 1-D thermodynamic ice growth model. To simulate the transition of surface height from the ice-free polynya to the distant ice that had a modal surface height of 0.26 m (Fig. 3), we modeled the ice growth at some distance from the polynya (Fig. 6b) and at Cape Jackson where polynya is observed (Fig. 6c). We used 4 cm mo^{-1} snow accumulation rate to reach a modest snow thickness of 14 cm at the end of winter that is reasonably close to 19±2 cm obtained with AMSR2 data for Peabody Bay (not shown). Based on this accumulation rate and no ocean heat flux, we estimate the end of winter ice thickness to be 1.3 m (Fig. 6b). Adding in the ocean heat flux lowers this thickness and also shifts the timing of maximum ice thickness. For instance, if the flux exceeded ~40 W m^{-2} the maximum ice thickness occurred in February and snow-ice formed after the surface flooded. Under the snow-free conditions and no heat flux, the ice thickness at the end of winter can reach about 1.7 m (Fig. 6c). For having ice-free water in May, the heat flux should reach 70 W m^{-2} and be above 200 W m^{-2} to let polynya form in early March (Fig. 6c).

The most important part of Fig. 6 is the last panel showing the surface heights of snow on the sea ice surrounding polynya under different combinations of snowfall rate and ocean heat flux. Under the assumption that the ocean heat flux in polynya is large (200 W m^{-2} or so) and keeps polynya is ice-free or covered with very thin ice with a small freeboard during the entire winter, these heights can be interpreted as the difference of surface heights between surrounding ice and polynya to mimic the spatial variations of ICESat-2 surface heights presented in Fig. 3. A set of model experiments allowed to find that maximum height difference at the end of winter of 0.36 m correspond to 0 W m^{-2} heat flux and snow accumulation rate of 12 cm mo^{-1} (Fig. 6d, black dash-dotted line). An insulating effect of snow at the higher accumulation rates does not allow ice to grow thick and, therefore, limits its freeboard considerably. However, smaller snowfall rates and modest heat fluxes may give flatter shape of surface heights in the end of growing season that is in a better agreement with the stable pattern of surface heights from March to May shown in Fig. 3. For instance, at 4 cm mo^{-1} and 10 W m^{-2} (solid red line) the modeled surface heights are around 0.20 m in April.

https://doi.org/10.5194/os-2022-16
Preprint. Discussion started: 1 April 2022

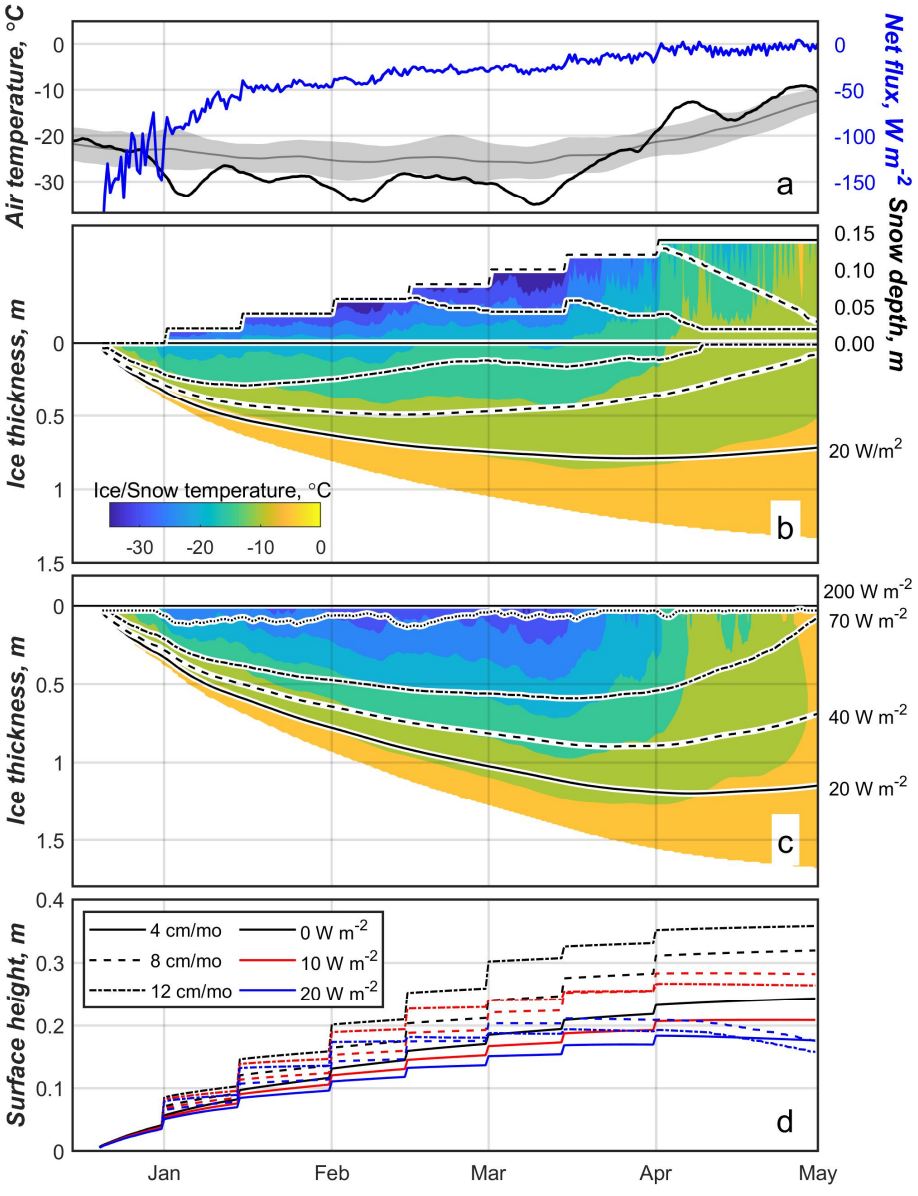

Figure 6: (a) The 2 m air temperature (black) and the net surface heat flux (blue). Grey line and shading indicate the mean 1979-2020 temperature and standard deviation. (b) The modeled evolution of ice/snow temperature and thickness in the vicinity of polynya under a constant snowfall rate of 4 cm/month (corresponding to 14 cm of snow pack at the end of March). (c) The same, but under no-snow conditions – a proxy of open water polynya area. Black lines in panel (b) and (c) show the evolution of ice and snow thicknesses if a steady ocean heat flux of 20 (solid), 40 (dashed), 70 W/m^2 (dash-doted) or 200 W/m^2 (doted) is added. (d) The difference between the sea level in polynya and surface heights of surrounding ice for different snow accumulation rates and ocean heat fluxes.

3.4. Ocean circulation and thermohaline structure in Kane Basin

To understand the physical mechanisms responsible for thinner ice in northwestern Peabody Bay and the polynya at Cape Jackson, we took advantage of the hi-resolution modelling of Nares Strait circulation and thermohaline structure conducted using the FESOM-2 model. According to the model results, the ocean circulation in Nares Strait consists of three patterns (Fig. 7a, b). The first one is the southward flow from the Lincoln Sea through the Robeson and Kennedy Channels and then along the western coast

https://doi.org/10.5194/os-2022-16
Preprint. Discussion started: 1 April 2022

of Kane Basin. This flow occupies the entire water column and consists of 3 distinctive layers; i) cold brackish polar mixed water within the upper 50-60 m, ii) the cold halocline observed at 70-90 m that separates surface mixed layer from (iii) relatively warm underlying modified Atlantic Water (mAW) which originated in the North Atlantic and was transported a long way from Fram Strait into the AO and to Northern Greenland (e.g. Melling et al., 2001). In Fig. 7a-b, this flow is shown with blue streamlines. The second pattern, shown in red color, is associated with the northward-flowing subsurface current at the eastern side of Smith Sound. A branch of this flow recirculates in the southern Kane Basin and merges with the southward jet, but another branch heads north along the Greenland slope toward Peabody Bay (Fig. 7b). This current is also associated with a penetration of relatively warm mAW, but from northern Baffin Bay. The third allocated pattern is associated with a cyclonic gyre in Peabody Bay (shown with green color in Fig. 7a, b).

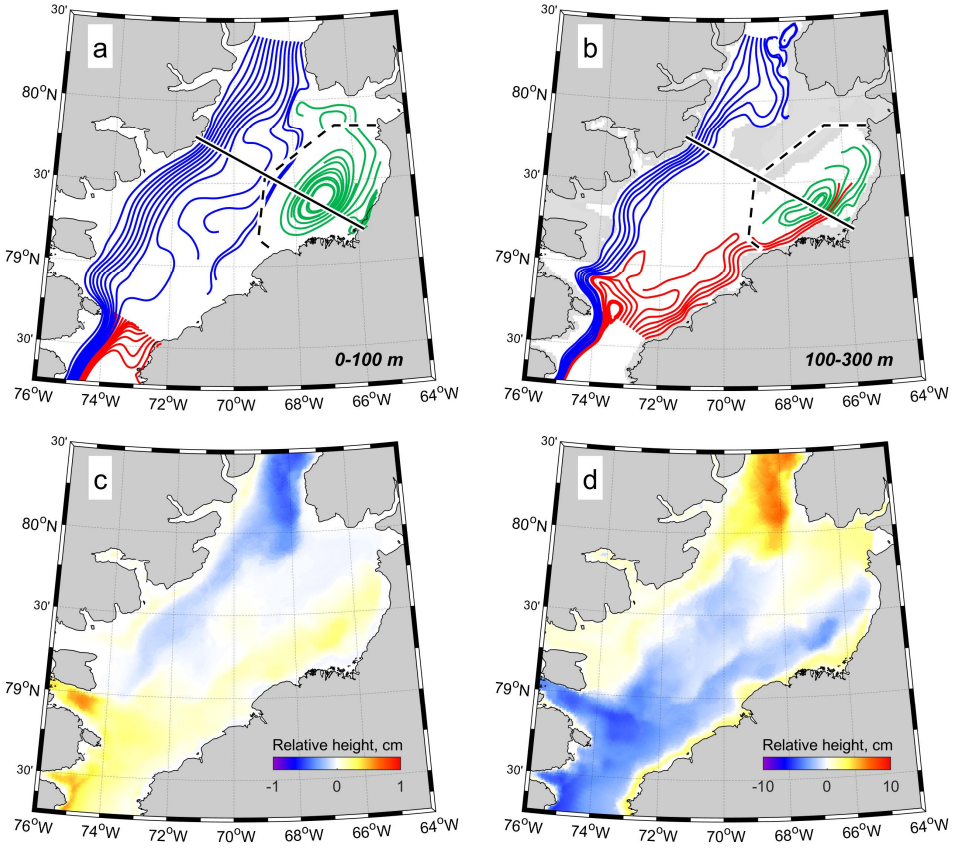

Figure 7: (a-b) The trajectories of water parcels calculated from the mean 2006-2010 model current velocities averaged within 0-100 m and 100-300 m, respectively. The blue, red and green lines correspond to three main circulation patterns in the region (see more details in the text). The black dashed line envelopes the region used for vorticity calculation (Figure 8) and the solid line shows the position of transect presented in Figure 9. The shaded area in panel (b) corresponds to the regions shallower than 150 m. The spatial distribution of the mean winter (November-June) thermo- and halosteric sea-level anomalies is shown in (c) and (d), respectively.

The model does not incorporate directly the formation of landfast ice, but it implicitly reproduces bridge formation via a cessation of ice motion through the strait. The average speed of ice drift in the main channel becomes less than 2 cm s^{-1} from December to May (Fig. 8a). In Peabody Bay, drift speeds are generally weaker compared to the main channel and an analog of landfast ice is observed there between November-December and June (Fig. 8a). Although the average duration of the observed ice bridges in

https://doi.org/10.5194/os-2022-16
Preprint. Discussion started: 1 April 2022

Nares Strait (between 20 January and 28 June; Vincent, 2019) is shorter than that predicted with the model, we may use December-June model data to describe the ocean circulation and thermohaline structure in the water column beneath the ice bridge. Furthermore, the model fails to reproduce no-bridge situations for winters 2006/07, 2008/09 and 2009/10. This discrepancy could be attributed to a critical impact of rheology and physical characteristics of the ice on bridge formation and the inability of the model to predict ice consolidation from a simple set of favorable atmospheric and oceanic conditions (Kirillov et al., 2021). However, considering the main goal of this study, we can disregard this failure and use the model-derived parameters during winter to describe the state of the ocean beneath the ice bridge.

The cessation of drift in winter leads to a considerable modification of the ocean circulation in Kane Basin. The virtual presence of the ice bridge causes a shift of the southward jet core from the surface to approximately 100 m (Fig. 9a, b). Such behavior is in a good consistence with observations reported in Rabe et al. (2012) and other models (Shroyer et al., 2015). In Peabody Bay, the seasonal change of circulation is more pronounced. The cyclonic gyre occupying the entire water column within this region in summer weakens significantly and even reverses to anticyclonic circulation at the surface during winter (Fig. 9a, b). Although the modeled sea ice in the bay becomes immobilized in November, the summer gyre remains strong until December (Fig. 8b).

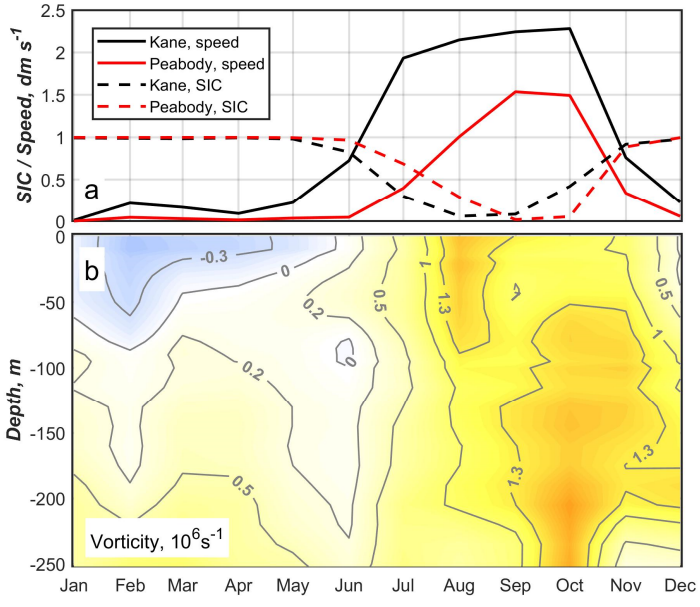

Figure 8: (a) The mean monthly SIC (dashed lines) and drift speeds (solid lines) within the main channel of Kane Basin (black) and in Peabody Bay (red). (b) The seasonal evolution of mean 2006-2010 vorticity within Peabody Bay. Both datasets are calculated from FESOM data.

The seasonal changes in temperature and salinity are mainly observed at shallow depths above 100 m. Below this depth, both parameters can be considered stable with no significant seasonal changes (Fig. 9c, d). The mAW penetrating to Kane Basin from the north is approximately 0.2-0.3 °C warmer compared to the southern branch from Baffin Bay (+0.12 vs -0.15 °C). This difference is also evident from historic observational data, but the confidence of those measurements is not very high because of a high spatio-temporal irregularity of observational data. All temperature profiles in Peabody Bay were obtained during summer and only a few measurements were made concurrently with observations in the main channel. Since a key intention of this research was to bring up the phenomenon of the sensible heat polynya in the middle of the ice bridge in Nares Strait and to discuss potential driving

https://doi.org/10.5194/os-2022-16
Preprint. Discussion started: 1 April 2022

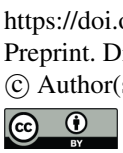

mechanisms, we limited the analysis of thermohaline state of water in the strait by model outputs that agree reasonably well with the observational data. A more detailed description of Kane Basin hydrography based on in-situ measurements can be found in Moynihan (1972), Sadler (1976), Bourke et al. (1989), Jones and Eert (2004), Rabe et al. (2010), and Münchow et al. (2011). The most up-to-date status of temperature measurements in Kane Basin can be found in Rignot et al. (2020) where the authors used historical temperature profiles to discuss the oceanic influence on the retreat of the Humboldt glacier.

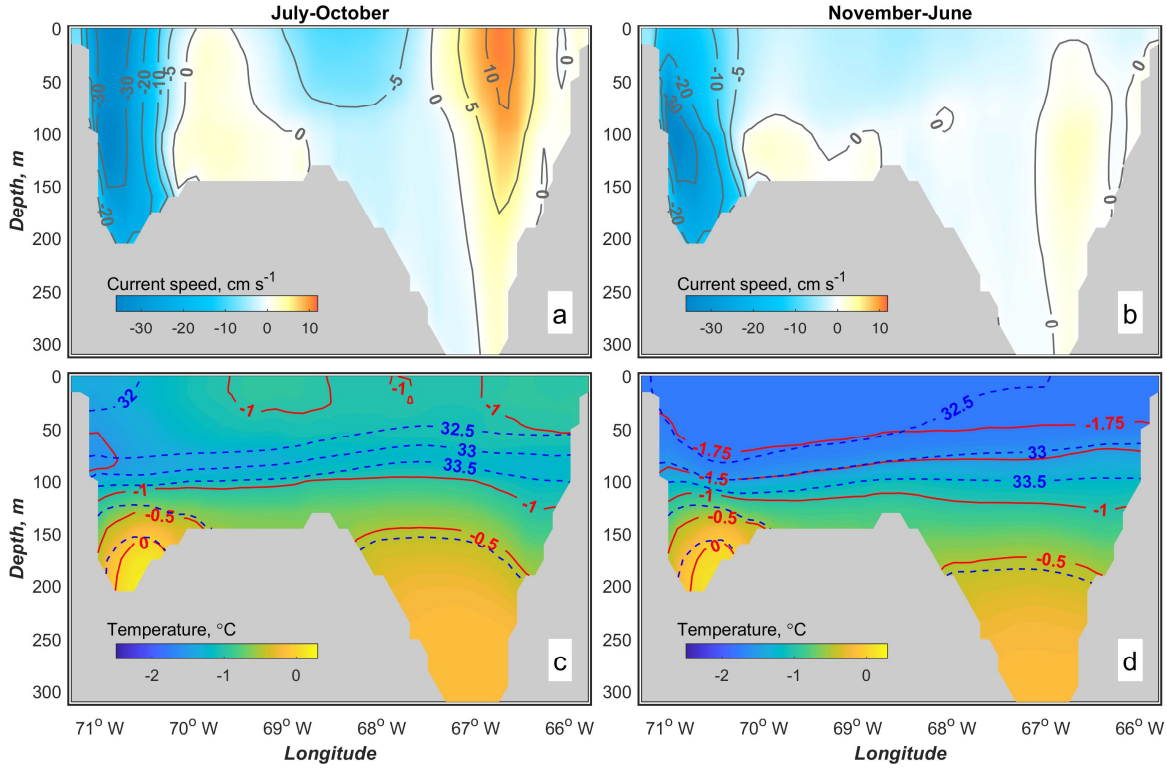

Figure 9: The modeled mean 2006-2010 summer (mobile ice) and winter (ice bridge) cross-sectional current speed (a, b) and water temperatures and salinities (c, d) at the transect across the central Kane Basin. Positive speeds correspond to northward flow.

While analyzing ATL07 data, it is also important to know if horizontal variations of temperature and salinity could affect the observed anomalies of surface heights. The spatial anomalies of thermosteric and halosteric heights in Nares Strait were calculated from FESOM2 temperature and salinity data similarly to an approach used in Volkov et al. (2013). It was found that temperature has predictably low impact on the steric heights in this area. The thermosteric anomalies caused by the horizontal variations of water temperature in Nares Strait do not exceed ±1 cm, but in Peabody Bay they are even smaller (Fig. 7c). The halosteric anomalies are generally an order of magnitude higher, but the difference between northwestern and southeastern Peabody Bay is also small and accounts for 3-4 cm only (Fig. 7d).

https://doi.org/10.5194/os-2022-16
Preprint. Discussion started: 1 April 2022

4. Discussion

4.1. The formation of ice thickness anomalies in Peabody Bay and polynya at Cape Jackson

The sea ice in Peabody Bay during winter is mainly represented by a smooth thermodynamically grown landfast ice cover with sporadic inclusions of ridges in the southern part of the bay (Fig. 4). The landfast ice typically starts to form in the bay in October, but in the northwestern bay, it remains unstable until ice bridge formation in December or even later dates in some years. As a result, the area in the vicinity of Cape Jackson is often found covered with thin mobile ice or even ice-free. This anomaly is further developing into a visible, or 'invisible' (Melling et al, 2015), polynya after the formation of the ice bridge in the southern Kane Basin and following immobilization of ice in the main channel.

According to altimetry data along the individual ICESat-2 tracks crossing the polynya in 2020 and 2021, the modal height of sea ice (including snow on the top of ice) surrounding the polynya was 0.26 m above the sea level (Fig. 3). The analysis of the spatial height anomalies ($\tilde{h}$) showed that maximal negative anomalies of 0.10-0.15 m are observed along the entire northern coast of Peabody Bay including polynya area (Fig. 4a-c). Over the rest of the bay, $\tilde{h}$ varies within relatively modest range between -0.05 and 0.05 m, but it forms the apparent pattern with mainly negative anomalies in the northwestern and positive anomalies in the southeastern parts of the bay. This pattern was highly pronounced in 2019 and 2020, but less evident in 2021 (Fig. 4a-c) which could be associated with an altered ocean heat flux limiting ice growth in certain regions. The brightness temperatures, T_b, shown in Figure 10 supports such suggestion of altered surface conditions. In December 2019 (Figure 10b), the higher T_b conditioned the ice-free (or covered with thin ice) area around Cape Jackson. Although the signatures of warmer water can also be traced along the eastern side of Kennedy channel in December 2018 and 2020, T_b was observed to be generally lower. Of course, the difference in temperatures presented in these snapshot images cannot explain the seasonally averaged height anomalies shown in Fig. 4. However, these differences demonstrate pronouncedly that there is significant interannual changeability of the ocean heat flux towards sea surface associated with either altering deep water temperature or water dynamics.

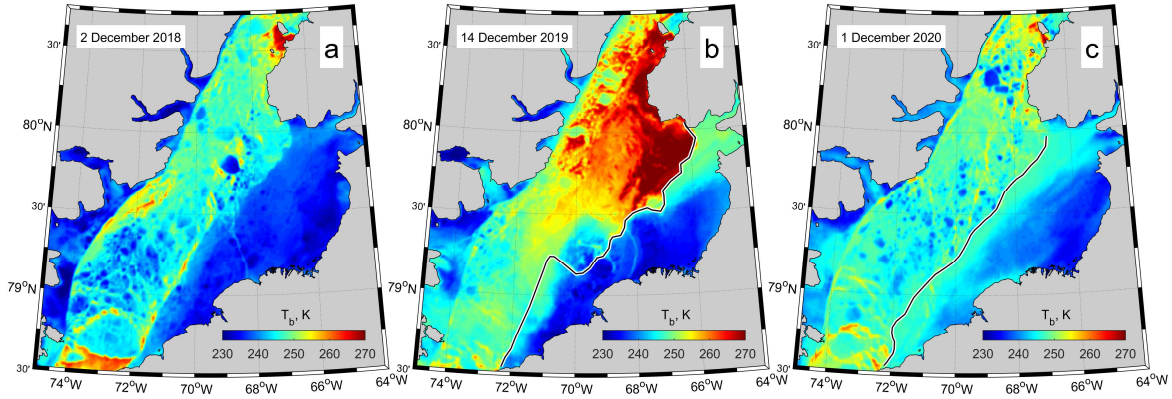

Figure 10: MODIS near clear-sky brightness temperatures on (a) 02 December 2018, (b) 14 December 2019 and (c) 01 December 2020. Images (b) and (c) show T_b several days prior to ice bridge formations in both years.

The steric anomalies in Peabody Bay are several times smaller than anomalies of ice surface heights (2-3 cm vs ~10 cm; Fig. 4a-c and Fig. 7d, respectively) and, therefore, seem to have negligible effect on $\tilde{h}$. In fact, extraction of mean steric anomalies from

https://doi.org/10.5194/os-2022-16
Preprint. Discussion started: 1 April 2022

405 $\tilde{h}$ would even increase the contrast of the latest between the northwestern and southeastern bay because of their generally opposite signs in these two regions. Although it confirms a confidence of the observed pattern of $\tilde{h}$, it is possible that an unknown spatial distribution of snow may considerably affect the magnitude of anomalies of ice freeboards and our suggestions about the ocean heat impact. Strikingly, to our knowledge, the only published values on in-situ measurement of snow and ice thickness at the end of winter was found in Dr. Kane's report and related to the southeastern part of Peabody Bay. The snow and ice thicknesses
410 measured during Dr. Kane's expedition were "*knee deep*" and "*seven feet five inches* [2.25 m]." (Kane, 1856; p.281). All available contemporary satellite-derived snow depth products suffer from missing data, low spatial resolution and large uncertainties limiting their practical usage for regional studies.

To investigate the effect of different snow depths and ocean heat flux on $\tilde{h}$ in the vicinity of polynya we used a 1-D ice growth model. Several simulations with different snow accumulation rates and ocean heat fluxes were run to find an optimal combination
415 of these parameters to match the absolute surface height of ~0.26 m obtained from ICESat-2. It was found that the ocean heat flux at Cape Jackson needed to exceed 200 W m^{-2} to open the polynya as early as in March. Such large heat flux seems to be associated with a direct upwelling of warm core of the southern branch of mAW rather than with vertical mixing. The results of modelling presented in Fig. 7a and Fig. 11 with streamlines heading northwest from Peabody Bay toward Kennedy Channel generally supports the upwelling hypothesis, although the highly uncertain bathymetry affect the confidence of the model results. With mAW being
420 topographically constrained within deep eastern part of Peabody Bay, given the ocean circulation it is plausible that AW may overrun the mid-basin ridge in certain areas to reach the surface.

The different combinations of the snow rates and ocean heat fluxes in the model give a wide range of surface heights within the ice surrounding the polynya (Fig. 6d). However, the best approximations of the target height of 0.26 m were obtained for the heat fluxes between 10-20 W m^{-2} and modest snow accumulation rate of 4-8 cm/mo that corresponds to 14-28 cm of snow accumulated
425 by the end of winter. Although there is no confident regional data on snow accumulation rate in Peabody Bay, this amount looks feasible as it envelops 14-24 cm snow depths (5-95% percentile range) in March-April obtained from daily AMSR2 data (not shown). The larger magnitudes of both parameters lead to eventual flooding and drop of height in the end of the winter season, whereas smaller fluxes and accumulation rates resulted in heights increasing with time that are not evident in the altimetry data (Fig. 3). Even though the model could reproduce the observed difference of surface height within landfast ice in vicinity of polynya
430 reasonably well, the obtained results should be considered only as an approximation because steady accumulation rates and heat fluxes were used, which is likely not representative of true snow cover evolution. A temporal variability of heat transport into the surface layer near Cape Jackson, for instance, can be expected based on the observed interannual variations in brightness temperatures (Fig. 10) and in the seasonal changes of cyclonic circulation within Peabody Bay (Fig. 8).

https://doi.org/10.5194/os-2022-16
Preprint. Discussion started: 1 April 2022

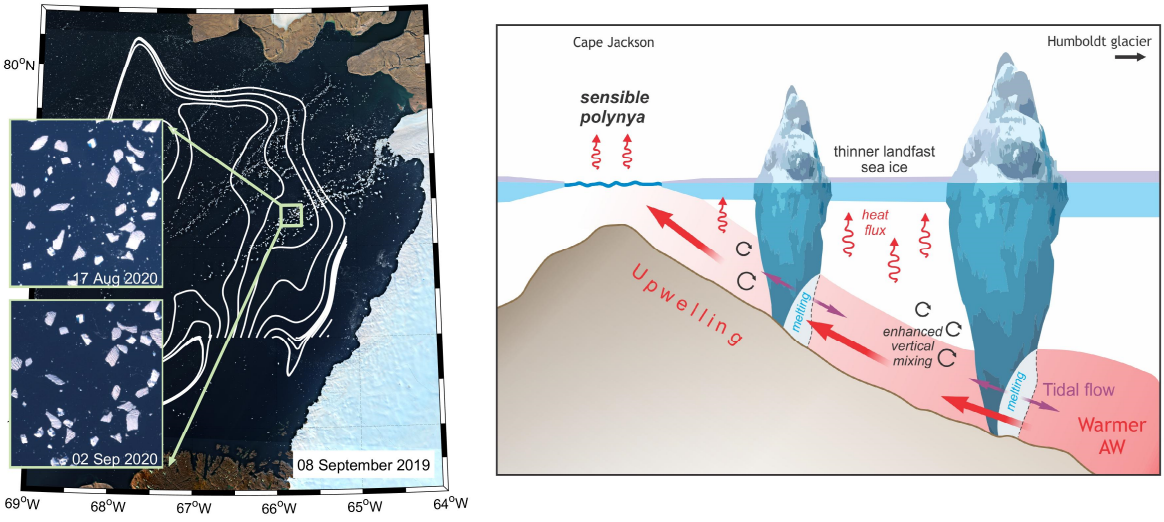

Figure 11: (left) The grounded icebergs in Peabody Bay. The white trajectories represent the mean November-June ocean circulation at 80 m depth from FESOM model. (right) The principle scheme of interaction of AW with a slope and grounded icebergs.

The only available source of ocean heat in Kane Basin during winter is associated with the relatively warm modified Atlantic Water penetrating into the basin from Lincoln Sea (northern branch) and from Baffin Bay (southern branch). Although the northern branch is warmer and, being considerably faster, transports more heat compared to the southern branch, the water temperature of the southern branch is also above the freezing point. According to FESOM2 simulations, the mean temperature of the mAW core in the central Peabody Bay is -0.15 °C or ~1.75 °C above freezing with a maximum observed at depth below 200 m. This heat may be either upwelled to the surface (leading to formation of sensible heat polynya at Cape Jackson) or transported upward by vertical mixing. Although the mean water dynamics in the bay during winter is relatively weak compared to the main channel (Fig. 9b), the strong semidiurnal tides in Nares Strait may play a critical role in vertical mixing through benthic stresses and shear instabilities (Davis et al., 2019). An additional factor facilitating vertical heat exchange in Peabody Bay is associated with the presence of hundreds of icebergs originated from Humboldt glacier. In satellite images, these icebergs are seen to form well-separated parallel chains oriented from NE to SE (Fig. 4f, Fig. 11). When comparing sequential images, it was seen that most of the icebergs comprising the chains were grounded and experienced little motion and/or rotation (insets in Fig. 11). The icebergs in the first glacier chain are stranded on the ~250 m isobath, corresponding to the draft of the tabular icebergs calved from the glacier to the north (Rignot et al., 2020). Further northwest, the grounded iceberg sizes become smaller and their chains are seen to form on shallower isobaths (i.e. icebergs also become thinner). Two other pronounced chains were estimated to be sitting at 150 m and 90 m isobaths, although there are more chains forming smaller clusters in between. Unfortunately, the high uncertainty of bottom topography in Peabody Bay does not support a better analysis.

However, it is noteworthy that all these iceberg chains are located within the region with pronounced negative anomalies of ice surface heights in 2019 and 2020. We suggest that, in combination with strong semidiurnal tidal currents, the grounded icebergs play a role in enhancing vertical mixing of warmer mAW at depth and also in melting their bases. Although the near-bottom water temperatures in Peabody Bay are negative, they are above in-situ freezing point providing necessary heat to melt the freshwater glacial ice (Loewe, 1961). However, the melting in this case is associated not with latent heat flux from water, but with dissolution controlled by solute transfer between water and ice-ocean interface (Woods, 1992). The rate of melting controlled by dissolution

https://doi.org/10.5194/os-2022-16
Preprint. Discussion started: 1 April 2022

is suggested to be low, although there is a certain lack of lab and nature experiments related to the melting of fresh ice in the salt water at temperatures below 0 °C but above freezing point. The base melting of icebergs might also explain why they form several well-separated chains over the mid-basin ridge. If icebergs had melted mainly from the surface during a relatively short summer, they would have gradually lost their mass and draft. As a result, they would have slowly ploughed northwest by the cyclonic gyre. Taking into account that surface melt may vary from berg to berg depending on their shapes and sizes, the draft changes would be different too and a random distribution of bergs would prevail in the area. But if the bottom melt exceeds the surface mass loss, the net buoyancies of grounded bergs decrease, and they get stranded even more with time. Opposite to the surface melt, the bottom melt goes all year round. At some point, the bottom part of iceberg contacting with warm water becomes too narrow to support the weight of ice above and the iceberg cracks. As a result, the iceberg height changes abruptly and it drifts to the next isobath corresponding to its new draft. Schematically, the described process is shown in Fig. 11. If the loss of bottom part occurs in winter, the iceberg starts to drift in followed summer. Assuming that the near-bottom melt (or dissolution) is likely a slow process, it may take longer than one season for an individual iceberg to crack.

4.2. The formation of ice thickness anomalies along the western coast of Nares Strait

The along-track anomalies of surface heights in Nares Strait shown in Fig. 4b and 4c also revealed the narrow (about 10 km wide) wedge of negative anomalies spreading over 200 km along the western coast of Nares Strait from Cape Frazer at south to the Hall Basin at north. At first glance, these observations contradict Ryan and Münchow (2017) who reported on the presence of thicker ice near Ellesmere Island (mean draft of 1.33 m) compared to the Greenlandic side (0.88 m) in Kenney Channel, based on upward-looking under-ice sonar data. Although Ryan and Münchow's results are consistent with an Ekman-layer response of the surface ocean and sea ice to local winds from the north, the authors considered only the periods of mobile sea ice when the potential impact of ocean heat on individual ice floes is relatively small due to their fast passage through the channel. However, a persistently enhanced ocean heat flux (even if small) beneath the ice bridge may play a great role in restricting ice growth near Ellesmere Island during winter. We suggest that the observed negative anomalies are attributable to the heat upwelled from the underlying mAW. The temperature in the northern branch of mAW in Kane Basin is about 0.3 °C higher compared to the temperature in the southern branch (Fig. 9c, d). In combination with higher current velocities within the subsurface jet (Fig. 9a, b) this would result in increased shear instabilities within the flow and higher upward heat flux that may have considerably stronger impact on ice growth compared to the northwestern Peabody Bay.

https://doi.org/10.5194/os-2022-16
Preprint. Discussion started: 1 April 2022

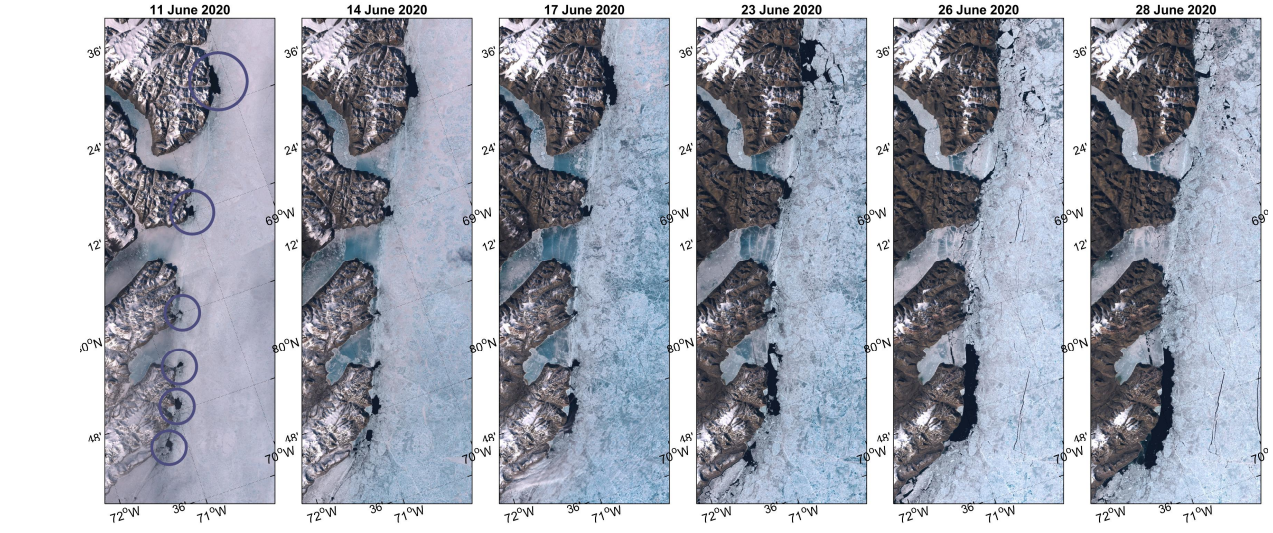

Figure 12: The series of Sentinel-2 images showing the evolution of polynyas along western coast of Kane Basin from the first appearance until the start of bridge collapse in June 2020. The circles in the left panel indicates the regions where open water polynyas first appear.

Although the anomalies along Ellesmere Island are comparable or even exceed those observed in the bay (Fig. 4b, c), they are not accompanied by higher surface temperatures at the end of winter (Fig. 5b, c). The absence of the temperature contrast, however, can be attributed to a generally thicker ice cover in the main channel comprising a large portion of MYI, whereas the ice in Peabody Bay mainly consists of FYI or may be covered with less snow (or a combination of these two factors). The stronger vertical mixing associated with the shear instability of the subsurface southward jet along the western coast is also supported by the fact of forming the chain of polynyas at the end of spring, shortly before a collapse of ice bridge. In 2020, for instance, the western polynyas started to open in early June (Fig. 12), whereas the landfast ice in Peabody Bay remained solid (except the polynya at Cape Jackson) until the bridge break up in the very end of June.

Unfortunately, the lack of in-situ measurements does not allow us to quantify the vertical oceanic heat fluxes to the western Nares Strait polynyas, but it is likely that the semidiurnal tide greatly affects the intensity of this process. The magnitude of barotropic tidal currents in Nares Strait is comparable with the speed of the mean southward flow (Münchow, 2016; Davis et al., 2019). Transformation of these currents over steep topography generates baroclinic semidiurnal tidal wave that may considerably enhance vertical mixing through benthic stresses and shear instabilities (Davis et al., 2019). From this perspective, the fact that most of the western polynyas first appear near prominent headlands (Fig. 12) generally support the idea of topographically controlled instabilities associated with the mean current and reversible tidal flow. When considering the tide's effect on the formation of sensible heat polynyas in Nares Strait, we note in particular the inland polynya in Flagler Bay, which is located in the south-western part of the strait (Hannah et al., 2009). The Flagler Bay polynya is located about 40 km from the main channel and, therefore, the tide must be the main forcing factor responsible for the maintenance of open water, probably through the local upwelling over the sill at the entrance to the bay.

Despite the extensive evidence from true-color satellite imagery, a more detailed analysis of polynyas in western Nares Strait remains difficult. A relatively short cross-shore extension of polynyas and the short period of their existence do not allow us to use the ICESat-2 altimetry similarly to what was done for polynya at Cape Jackson. The western polynyas are simply bypassed by the relatively sparse along-track ATL07 data with their low repeat rate. Without a reference level, we were furthermore not able to use

https://doi.org/10.5194/os-2022-16
Preprint. Discussion started: 1 April 2022

the ice growth model for estimation of absolute ice/snow surface heights within the wedge of negative anomalies along Ellesmere Island similarly to how it was done in Section 4.3.

4.3. The role of thinner ice in Kane Basin in ice bridge break-up

The break-up of the ice bridge in Nares Strait is a complex process that may be determined by a number of factors (Vincent & Marsden, 2001; Kirillov et al., 2021). A certain combination of wind forcing, spring-neap tidal cycle and ice type composition is believed to determine the timing of ice bridge break-up, similarly to the bridge formation process (Kirillov et al., 2021). Based on the results presented here, we propose that thinner coastal ice, formed under conditions of enhanced oceanic heat flux from mAW, weakens the cohesion of landfast ice against the shoreline in Kane Basin and also facilitates an earlier ice bridge break-up comparing to a supposed no-polynyas situation. The impact of ocean heat on ice growth in the coastal zones is clearly evidenced in the series of satellite images in Fig. 13 and Fig. 14 that show the gradual development of the polynya at Cape Jackson during spring 2020. The polynya was generally well-constrained during March-May. However, in late May, the polynya started to increase in size, reached its maximum extension in mid-June, and finally broke up around 22 June (Fig. 14a, b). This break-up appeared to release internal stresses in the ice bridge and led to concomitant ice cover break-ups in the main channel. On 26 June, the still consolidated landfast ice in the main channel lost its cohesion with the western coastline and began to shift slowly southward. This movement began while the bridge was still in place, but large pieces of the ice bridge cover began breaking apart along the southern arch (Fig. 14c). A complete collapse of the ice bridge occurred a few days later around 1 July 2020.

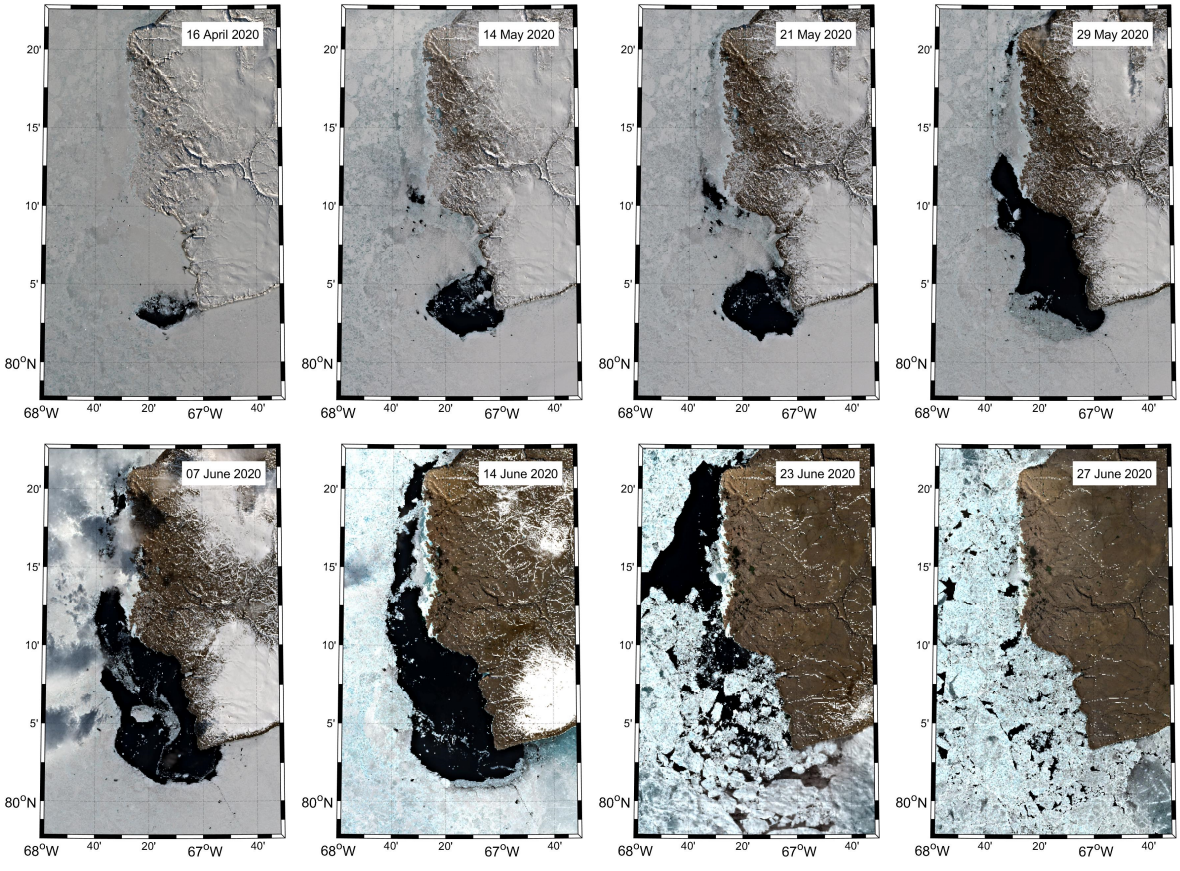

https://doi.org/10.5194/os-2022-16
Preprint. Discussion started: 1 April 2022

Figure 13: The evolution of polynya at Cape Jackson from April to June 2020 from Sentinel-2 data.

Although our hypothesis that visible and invisible (i.e., thin ice areas) polynyas facilitate ice bridge break-up in Nares Strait is speculative, we would like to emphasize the observations that the first movements of the immobilized ice cover occurred in areas with negative ice thickness anomalies during winter and where polynyas are observed. The critical role of the ocean heat flux in formation of these areas is underlined by the fact of the existence of the sensible polynya in the center of the ice bridge. The only oceanic heat source available to maintain such a polynya through winter is the modified Atlantic Water. The warming of mAW in front of Humboldt glacier by 0.9 °C since 1961 reported by Rignot et al. (2021) may indicate a continuing increase of ocean thermal impact, although the existing spatial heterogeneity of data limited by summer period make the estimated trend highly uncertain. However, based on the more consistent mooring data in Kennedy Channel, Münchow (2011) reported a very similar warming in the southward branch of mAW of 0.23 °C/decade. Considering that all five winters when the ice bridge in Nares Strait failed to form occurred during the last 15 years (i.e., 2007, 2009, 2010, 2017 and 2019), we suggest that the mechanisms associated with ocean heat in weakening the ice bridge ice cover will make the existence of the ice bridge increasingly vulnerable as climate change and further warming of mAW progresses. However, presently a quantitative estimate of the ocean thermal impact on the bridge stability can be only accomplished with coupled ice-ocean models incorporating a comprehensive ice rheology or sea ice dynamics model (e.g. Plante et al., 2020; West et al., 2021), which is beyond the scope of this study.

https://doi.org/10.5194/os-2022-16
Preprint. Discussion started: 1 April 2022

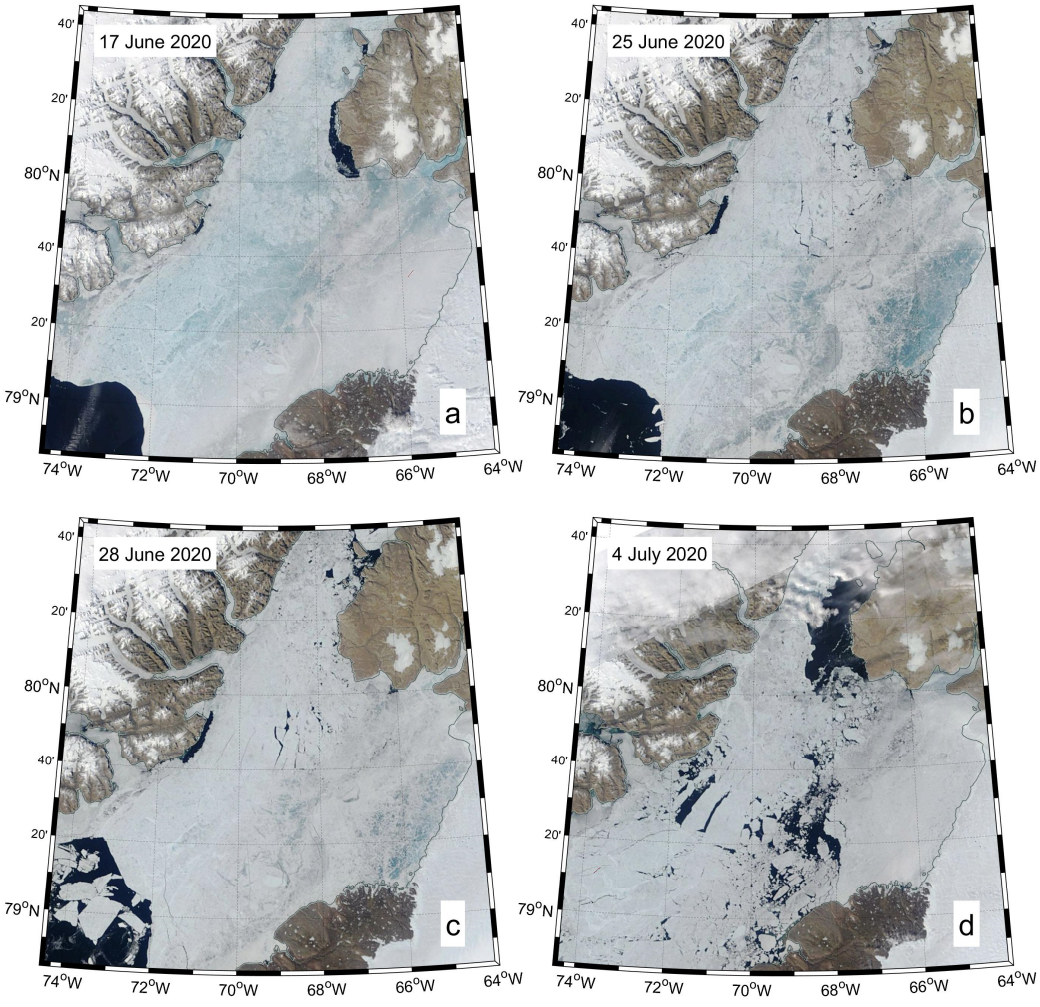

Figure 14: The process of the ice bridge break-up in June 2020 in MODIS true-color imagery.

5. Summary

This paper present insights into the ice-ocean interaction beneath the ice bridge in Nares Strait. The research was motivated by the fact that a sensible heat polynya has been observed via remote sensing in the center of the ice bridge (at Cape Jackson) every winter. In fact, our research is standing on the shoulders of Dr. Elisha Kane who discovered open water at Cape Jackson and expressed an opinion that "… *ocean-currents may exert on the temperature of these far-northern regions* [and keep water ice-free]" (Kane, 1856; p. 309). To examine Dr. Kane's enlightened suggestion, we used a combination of remote sensing data, and results from hi-resolution FESOM2 oceanic circulation model and 1-D ice growth model. The ICESat-2 altimetry demonstrates that the polynya at Cape Jackson is a part of a much broader area in the northwestern Peabody Bay forming negative ice thickness anomalies during both ice-bridge and no-bridge winters. These anomalies are likely associated with the upward heat flux from the relatively warm modified Atlantic Water penetrating to Kane Basin through Smith Sound and circulating cyclonically at depth within Peabody Bay. Using the observed mode of absolute surface heights around the polynya (0.26 m) as a target elevation, we

https://doi.org/10.5194/os-2022-16
Preprint. Discussion started: 1 April 2022

ran a series of simulations of ice growth with different combination of the snow accumulation rates and ocean heat fluxes. In simulations of anomalous ice thicknesses, the best match was obtained using a relatively modest heat flux of 10-20 W/m^2 and snow accumulation rates of 4-8 cm/mo, although there might be a large uncertainty associated with possible seasonal changeability in both variables. We suggested that the vertical mixing and upward heat flux of mAW in the northwestern Peabody Bay could be enhanced by the presence of dense chains of icebergs, calved from Humboldt glacier, that have become grounded on the eastern slope of the mid-basin ridge in Kane Basin. The interaction of these icebergs with the mean and tidal currents may function as an efficient stirring machine. However, the maintenance of open water at Cape Jackson throughout winter requires much stronger ocean heat flux of at least 200 W/m^2. Such high heat flux is thought to be associated with a direct upwelling (as a result of convergence of the mean flow over slope) rather than with vertical mixing.

Another prominent zone with negative surface height anomalies was revealed along the western side of Kane Basin and Kennedy Channel. This narrow (~10 km) zone spreads over 200 km along the coast of Ellesmere Island from Cape Frazer in the south to the Hall Basin in the north and turns into the system of coastal polynyas that form several weeks prior to the ice bridge break-up. The ice thickness anomalies along the western coast were considered to be associated with heat released from the northern branch of mAW that carry relatively warm water in the subsurface layer southward from Lincoln Sea. The jet of this flow follows along the western slope of the strait during winter, which might enhance shear instabilities over a steep topography and vertical mixing. Modelling results suggest that the northern branch of mAW in Kane Basin is considerably faster and slightly warmer compared to the Baffin Bay branch, which indicates the possibility of a larger vertical heat flux than the estimated 10-20 W/m^2 in the northwestern Peabody Bay. However, obtaining a specific number is not possible without in-situ measurements.

As a result of the ocean heat flux, the extended areas with considerably thinner ice form along the northern and western coasts of Kane Basin at the end of winter. Based on comparison with the stages of the Nares Strait ice bridge collapse in 2020, we proposed that these thin or reduced ice areas could weaken the stability of ice bridge and promote its earlier collapse in summer. Moreover, the prospect of further amplification of ocean heat fluxes, due to increases of the temperature of inflowing modified Atlantic Water linked to climate warming, is expected to further impact the stability of ice bridge in Nares Strait or its formation altogether.

Data availability

All satellite data used in this research were obtained from open sources. ICESat-2 ATL07 data is available from National Snow & Ice Data Center (https://nsidc.org/data/atl07) as well as AMSR sea ice brightness temperatures and snow depths (https://nsidc.org/data/AU_SI6/versions/1). The MODIS true color imagery and band-31 sea surface brightness temperature were obtained through NASA's Worldview application (https://worldview.earthdata.nasa.gov), part of NASA's Earth Observing System Data and Information System (EOSDIS). The optical Sentinel-2 images are available from the Copernicus Open Access Hub (https://scihub.copernicus.eu/dhus). The FESOM2 model source code and configuration files are available from https://github.com/FESOM/fesom2. The portion of 1km-resolution FESOM2 data used for this research can be found at https://doi.org/10.5281/zenodo.6360063.

Author contributions

SK designed this research, generated all figures and performed the majority of data analysis. ID, DBabb, JE, SR, DJ and DBarber contributed to data analysis and developing of the research concept. The original manuscript was drafted by SK and further revised and edited by ID, DBabb, JE, SR, DJ, NK and DBarber. NK provided the results of high-resolution FESOM2 model for Nares Strait region. All authors have read and agreed to the published version of the manuscript.

https://doi.org/10.5194/os-2022-16
Preprint. Discussion started: 1 April 2022

Competing interests

The authors declare that they have no conflict of interest.

Acknowledgements

Funding for this work was mainly provided by the Canada Excellence Research Chair (CERC) program (D. Dahl-Jensen, PI). D. Babb, J. Ehn, S. Rysgaard and D. Barber are supported by the Natural Sciences and Engineering Research Council (NSERC) of Canada. D. Babb is additionally supported by the Canadian Meteorological and Ocenographic Society (CMOS). The authors thank National Snow and Ice Data Center for the ICESat-2 data on sea ice heights (https://nsidc.org/data/ATL07/versions/3). We acknowledge the use of MODIS data and imagery available from NASA's Worldview application (https://worldview.earthdata.nasa.gov), part of NASA's Earth Observing System Data and Information System (EOSDIS). This work is a contribution to the Arctic Science Partnership (ASP) and ArcticNet.

References

Babb, D., Kirillov, S., Kuzyk, Z., Netser, T., Liesch, J., Kamula, C. M., Zagon, T., Barber, D. G. and Ehn, J.: On the intermittent formation of an ice bridge (Nunniq) across Roes Welcome Sound, Northwestern Hudson Bay, and its use to local Inuit hunters, Arctic (in press).

Barber, D. G. and Massom, R. A.: The role of sea ice in Arctic and Antarctic polynyas, in Polynyas: Windows to the World, edited by W. O. Smith and D. G. Barber, Elsevier Oceanogr. Ser., 74, 1–54, 2007.

Barber, D. G., Babb, D. G., Ehn, J. K., Chan, W., Matthes, L., Dalman, L. A., Campbell, Y., Harasyn, M. L., Firoozy, N., Theriault, N., Lukovich, J. V., Zagon, T., Papakyriakou, T., Capelle, D. W., Forest, A. and Gariepy, A.: Increasing mobility of high Arctic sea ice increases marine hazards off the east coast of Newfoundland, Geophysical Research Letters, doi:10.1002/2017GL076587, 2018.

Beszczynska-Möller, A., Woodgate, R.A., Lee, C., Melling, H. and Karcher, M.: A synthesis of exchanges through the main oceanic gateways to the Arctic Ocean, Oceanography, 24(3), 82–99, doi:10.5670/oceanog.2011.59, 2011.

Bilello, M. A.: Formation, growth, and decay of sea-ice in the Canadian Arctic Archipelago, Arctic, 14(1), 2–24, 1961.

Bourke, R. H., Addison, V. G. and Paquette, R. G.: Oceanography of Nares Strait and northern Baffin Bay in 1986 with emphasis on deep and bottom water formation, Journal Geophysical Research, 94 (C6), 8289– 8302, doi:10.1029/JC094iC06p08289, 1989.

Cavalieri, D. J., Markus, T. and Comiso, J. C.: AMSR-E/Aqua daily L3 6.25 km 89 GHz brightness temperature polar grids, version 3. Boulder, Colorado USA. NASA National Snow and Ice Data Center Distributed Active Archive Center, doi:10.5067/AMSR-E/AE_SI6.003, 2014.

Danilov, S., Sidorenko, D., Wang, Q. and Jung, T.: The finite-volume sea ice–ocean model (FESOM2), Geoscientific Model Development, 10, 765–789, 2017.

Dumont, D., Gratton, Y. and Arbetter, T. E.: Modeling wind-driven circulation and Landfast Ice-Edge Processes during Polynya Events in Northern Baffin Bay, Journal Physical Oceanography, 40, 1356–1372, doi:10.1175/2010JPO4292.1, 2010.

Davis, P. E. D., Johnson, H. L. and Melling, H.: Propagation and vertical structure of the tidal flow in Nares Strait, Journal of Geophysical Research: Oceans, 124, 281–301, doi:10.1029/2018JC014122, 2019.

https://doi.org/10.5194/os-2022-16
Preprint. Discussion started: 1 April 2022

Glissenaar, I. A., Landy, J. C., Petty, A. A., Kurtz, N. T. and Stroeve, J. C.: Impacts of snow data and processing methods on the interpretation of long-term changes in Baffin Bay sea ice thickness, The Cryosphere, 15, 4909-4927, doi:10.5194/tc-15-4909-2021, 2021.

Hannah, C., Dupont, F. and Dunphy, M.: Polynyas and Tidal Currents in the Canadian Arctic Archipelago, Arctic, 62, 83-95, doi:10.14430/arctic115, 2009.

Hastrup, K., Mosbech, A. and Grønnow, B.: Introducing the North Water: Histories of exploration, ice dynamics, living resources, and human settlement in the Thule Region, Ambio, 47, 162–174, doi:10.1007/s13280-018-1030-2, 2018.

Hayes, I. I.: The open Polar sea: a narrative of a voyage of discovery towards the North pole, in the schooner "United States". New York, Hurd and Houghton, 1867.

Hersbach, H., Bell, B., Berrisford, P., et al.: The ERA5 global reanalysis, Q J R Meteorol. Soc., 146: 1999– 2049, doi:10.1002/qj.3803, 2020.

Ito, H.: Wind through a channel - surface wind measurements in Smith Sound and Jones Sound in Northern Baffin Bay, Journal of Applied Meteorology, 21, 1053–1062, 1982.

Jones, E. and Eert, A.: Waters of Nares Strait in 2001, Polarforschung, 74, 2006.

Kane, Elisha Kent: Arctic explorations: the second Grinnell expedition in search of Sir John Franklin, 1853, '54, '55, Vol. I, Philadelphia: Childs & Peterson, doi:10.5962/bhl.title.147879, 1856.

Kirillov, S., Dmitrenko, I., Babb, D., Rysgaard, S. and Barber, D.: The effect of ocean heat flux on seasonal ice growth in Young Sound (Northeast Greenland), Journal of Geophysical Research – Oceans, doi:10.1002/2015JC010720, 2015.

Kirillov, S., Babb, D. G., Komarov, A. S., Dmitrenko, I., Ehn, J. K., Worden, E., Candlish, L., Rysgaard, S. and Barber, D. G.: On the physical settings of ice bridge formation in Nares Strait, Journal of Geophysical Research: Oceans, 126, e2021JC017331, doi:10.1029/2021JC017331, 2021

Koldunov, N. V., Danilov, S., Sidorenko, D., Hutter, N., Losch, M., Goessling, H. and Jung, T.: Fast EVP solutions in a high-resolution sea ice model, Journal of Advances in Modeling Earth Systems, 11, 1269–1284, doi:10.1029/2018MS001485, 2019.

Kwok, R.: Variability of Nares Strait ice flux, Geophysical Research Letters, 32, L24502. doi:10.1029/2005GL024768, 2005.

Kwok, R. Toudal Pedersen, L., Gudmandsen, P. and Pang, S. S.: Large sea ice outflow into the Nares Strait in 2007, Geophysical Research Letters, 37, L03502, 2010.

Kwok, R., Cunningham, G., Markus, T., Hancock, D., Morison, J. H., Palm, S. P., Farrell, S. L., Ivanoff, A., Wimert, J. and the ICESat-2 Science Team: ATLAS/ICESat-2 L3A Sea Ice Freeboard, Version 3, ATL10, Boulder, Colorado USA. NSIDC: National Snow and Ice Data Center, doi:10.5067/ATLAS/ATL10.003, 2020a.

Kwok, R., Kacimi, S., Webster, M. A., Kurtz, N. T. and Petty, A. A.: Arctic snow depth and sea ice thickness from ICESat-2 and CryoSat-2 freeboards: A first examination, Journal of Geophysical Research: Oceans, 125, doi:10.1029/2019JC016008, 2020b.

Landy, J. C., Ehn, J. K., Babb, D. G., Thériault, N. and Barber, D. G.: Sea ice thickness in the Eastern Canadian Arctic: Hudson Bay Complex & Baffin Bay, Remote Sensing of Environment, 200, 281–294, doi:10.1016/j.rse.2017.08.019, 2017.

Lebedev, V.V.: Ice growth in the Arctic rivers and seas and its dependence on negative air temperatures, Arctic Proceedings, 5-6: 9-25, 1938.

Loewe, F.: On melting of fresh-water Ice in sea-water, Journal of Glaciology, 3(30), 1051-1052. doi:10.3189/S0022143000017457, 1961.

Meier, W. N., Comiso, J. C. and Markus, T.: AMSR-E/AMSR2 Unified L3 Daily 6.25 km Polar Gridded 89 GHz Brightness Temperatures, Version 1. Boulder, Colorado USA. NASA National Snow and Ice Data Center Distributed Active Archive Center, doi:10.5067/NX1R09ORNOZN, 2018.

675 Melling, H., Gratton, Y. and Ingram, G.: Ocean circulation within the North Water polynya of Baffin Bay, Atmosphere-Ocean, 39:3, 301-325, doi:10.1080/07055900.2001.9649683, 2001.

Melling, H., Haas, C. and Brossier, E.: Invisible polynyas: Modulation of fast ice thickness by ocean heat flux on the Canadian polar shelf, Journal Geophysical Research: Oceans, 120, 777– 795, doi:10.1002/2014JC010404, 2015.

Moore, G. W. K., Schweiger, A., Zhang, J. and Steele, M.: Spatiotemporal variability of sea ice in the arctic's last ice area,
680 Geophysical Research Letters, 46. doi:10.1029/2019GL083722, 2019.

Moynihan, M. J.: Oceanographic observations in Kane Basin, September 1968 and July-September 1969, U.S. Coast Guard Oceanographic Report No. 55, 70 p., 1972.

Münchow, A. and Melling, H.: Ocean current observations from Nares Strait to the west of Greenland: Interannual to tidal variability and forcing, Journal of Marine Research, 66, 801–833, doi: 10.1357/002224008788064612, 2008.

685 Münchow, A., Falkner, K., Melling, H., Rabe, B. and Johnson, H.: Ocean Warming of Nares Strait Bottom Waters Off Northwest Greenland, 2003–2009, Oceanography, 24, 114-123, doi:10.5670/oceanog.2011.62, 2011.

Münchow, A.: Volume and Freshwater Flux Observations from Nares Strait to the West of Greenland at Daily Time Scales from 2003 to 2009, Journal Physical Oceanography, 46, 141–157, doi:10.1175/JPO-D-15-0093.1, 2016.

Plante, M., Tremblay, B., Losch, M. and Lemieux, J.-F.: Landfast sea ice material properties derived from ice bridge simulations
690 using the Maxwell elasto-brittle rheology, The Cryosphere, 14, 2137–2157, doi:10.5194/tc-14-2137-2020, 2020.

Preußer, A., Ohshima, K. I., Iwamoto, K., Willmes, S. and Heinemann, G.: Retrieval of wintertime sea ice production in Arctic polynyas using thermal infrared and passive microwave remote sensing data, Journal Geophysical Research: Oceans, 124, 5503–5528. doi:10.1029/2019JC014976, 2019.

QIA (Qikiqtani Inuit Association): Sarvarjuaq and Qikiqtait: Inuit Stewardship and the Blue Economy in Nunavut's Qikiqtani
695 Region (Draft). Available at www.qia.ca. 37 p., 2020.

Rasmussen, K.: Greenland by the Polar Sea: the story of the Thule expedition from Melville Bay to cape Morris Jesup. London: William Heinemann, 1921.

Rostosky, P., Spreen, G., Farrell, S. L., Frost, T., Heygster, G. and Melsheimer, C.: Snow depth retrieval on Arctic sea ice from passive microwave radiometers—Improvements and extensions to multiyear ice using lower frequencies, Journal of Geophysical
700 Research: Oceans, 123, 7120-7138, doi:10.1029/2018JC014028, 2018.

Rabe, B., Münchow, A., Johnson, H. L. and Melling, H.: Nares Strait hydrography and salinity field from a 3-year moored array. Journal of Geophysical Research, 115, C07010, doi:10.1029/2009JC005966, 2010.

Rabe, B., Johnson, H. L., Münchow, A. and Melling, H.: Geostrophic ocean currents and freshwater fluxes across the Canadian polar shelf via Nares Strait, Journal of Marine Research, 70, 603–640, 2012.

705 Rignot, E., An, L., Chauche, N., Morlighem, M., Jeong, S., Wood, M., Mouginot, J., Willis, J.K., Klaucke, I., Weinrebe, W. and Muenchow, A.: Retreat of Humboldt Gletscher, North Greenland, driven by undercutting from a warmer ocean, Geophysical Research Letters, 48(6), doi: 10.1029/2020GL091342, 2021.

Ryan, P. A. and Münchow, A.: Sea ice draft observations in Nares Strait from 2003 to 2012, Journal of Geophysical Research: Oceans, 122, 3057– 3080, doi:10.1002/2016JC011966, 2017.

710 Sadler, H. E.: Water, heat, and salt transports through Nares Strait, Ellesmere Island, J. Fish. Res. Board Can., 33, 2286–2295, 1976.

Samelson, R. M., Agnew, T., Melling, H. and Münchow, A.: Evidence for atmospheric control of sea-ice motion through Nares Strait, Geophysical Research Letters, 33, L02506. doi:10.1029/2005GL025016, 2006.

Schledermann, P.: Preliminary results of archaeological investigations in the Bache Peninsula Region, Ellesmere Island, N.W.T., Arctic, 31(4): 459, 1978.

Schledermann, P.: Polynyas and Prehistoric Settlement Patterns, Arctic, V. 33, No. 2, p. 292-302, 1980.

Scholz, P., Sidorenko, D., Gurses, O., Danilov, S., Koldunov, N., Wang, Q. and Jung, T.: Assessment of the finite-volume sea ice-ocean model (FESOM2.0) - Part 1: Description of selected key model elements and comparison to its predecessor version, Geoscientific Model Development, 12, 4875–4899, 2019.

Shokr, M. E., Wang, Z. and Liu, T.: Sea ice drift and arch evolution in the Robeson Channel using the daily coverage of Sentinel-1 SAR data for the 2016–2017 freezing season, The Cryosphere, 14, 3611-3627, doi:10.5194/tc-14-3611-2020, 2020.

Shroyer, E. L., Samelson, R. M., Padman, L. and Münchow, A.: Modeled ocean circulation in Nares Strait and its dependence on landfastice cover, Journal of Geophysical Research: Oceans, 120, 7934-7959, doi:10.1002/2015JC011091, 2015.

Tamura, T. and Ohshima, K. I.: Mapping of sea ice production in the Arctic coastal polynyas, Journal of Geophysical Research, 116, C07030. doi:10.1029/2010JC006586, 2011.

Tedesco, M. and Jeyaratnam, J.: AMSR-E/AMSR2 Unified L3 Global Daily 25 km EASE-Grid Snow Water Equivalent, Version 1. Snow depth. Boulder, Colorado USA, NASA National Snow and Ice Data Center Distributed Active Archive Center. doi:10.5067/8AE2ILXB5SM6, 2019.

Tsujino, H., Urakawa, S., Nakano, H., Small, R. J., Kim, W. M., Yeager, S. G. and Yamazaki, D.: JRA-55 based surface dataset for driving ocean–sea-ice models (JRA55-do), Ocean Modelling, 130, 79–139, doi:10.1016/j.ocemod.2018.07.002, 2018.

Vibe, C.: The Marine Mammals and the Marine Fauna in the Thule district (Northwest Greenland) with Observations on Ice Conditions in 1939–41: Den Danske Thule og Ellesmere Land Ekspedition 1939–41. Meddelelser om Grønland, 150(6), Copenhagen: C. A. Reitzel, 1950.

Vincent, R.F. and Marsden, R.F.: An analysis of the dissolution of ice in Nares Strait using AVHRR Imagery, Atmosphere-Ocean, 39:3, 209-222, doi:10.1080/07055900.2001.9649677, 2001.

Vincent R.F.: A Study of the North Water Polynya ice arch using four decades of satellite data, Scientific Reports, 9, doi:10.1038/s41598-019-56780-6, 2019.

Volkov, D. L., Landerer, F.W. and Kirillov, S. A.: The genesis of sea level variability in the Barents Sea, Continental Shelf Research, 66, 92-104, doi:10.1016/j.csr.2013.07.007, 2013.

Wang, Q., Danilov, S., Jung, T., Kaleschke, L. and Wernecke, A.: Sea ice leads in the Arctic Ocean: Model assessment, interannual variability and trends, Geophysical Research Letters, 43, 7019–7027, doi:10.1002/2016GL068696, 2016.

Wang, Q., Koldunov, N. V., Danilov, S., Sidorenko, D., Wekerle, C., Scholz, P., et al.: Eddy kinetic energy in the Arctic Ocean from a global simulation with a 1-km Arctic, Geophysical Research Letters, 47, e2020GL088550. doi:10.1029/2020GL088550, 2020.

Warren, S. G., Rigor, I. G., Untersteiner, N., Radionov, V. F., Bryazgin, N. N. and Alexandrov, Y. I.: Snow depth on Arctic Sea ice. Journal of Climate, 12, 1814–1828, 1999.

West, B., O'Connor, D., Parno, M., Krackow, M. and Polashenski, C.: Bonded discrete element simulations of sea ice with non-local failure: Applications to Nares Strait. arXiv:2105.05143v2, doi: 10.1002/essoar.10507028.1, 2021.

Woods, A. W.: Melting and dissolving, J. Fluid Mech., 239, 429 – 448, 1992.